iScience

CellPress
OPEN ACCESS

Article

Spatiotemporal orchestration of macrophage activation trajectories by Vγ4 T cells during skin wound healing

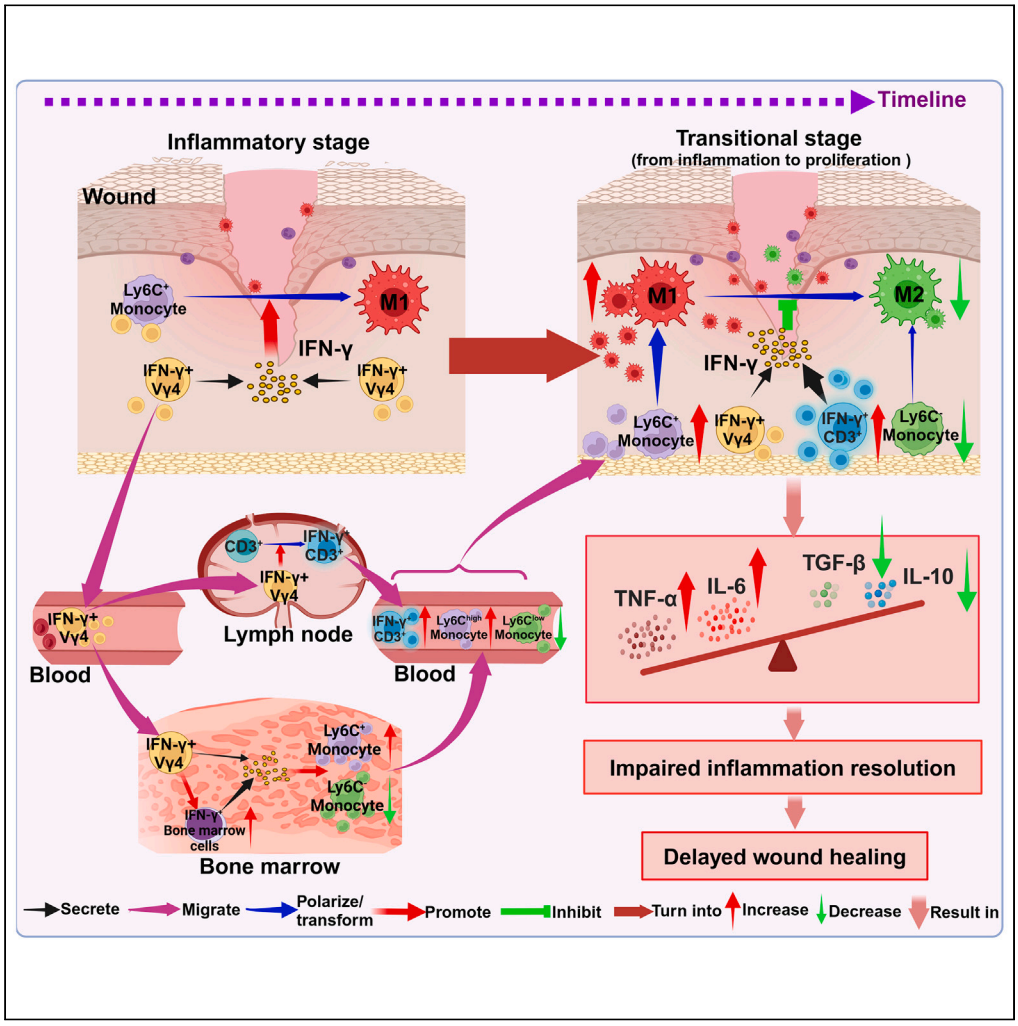

Wengang Hu, Xiaorong Zhang, Zhongyang Liu, ..., Jianlei Hao, Gaoxing Luo, Weifeng He

logxw@yahoo.com (G.L.)
heweifeng@tmmu.edu.cn (W.H.)

Highlights

Vγ4$^+$γδ T cells prolong inflammation via sustained M1 activation and M2 suppression

Local Vγ4$^+$γδ T cells in wounds mainly modulate macrophages polarization via IFN-γ

IFN-γ$^+$ lymphocytes promoted by infiltrating Vγ4$^+$γδ T cells enforce M1 programming

Infiltrated Vγ4$^+$ γδ T cells in bone marrow increases Ly6C$^+$ monocytes generation

Hu et al., iScience 27, 109545
April 19, 2024
https://doi.org/10.1016/j.isci.2024.109545

iScience

CellPress
OPEN ACCESS

Article

Spatiotemporal orchestration of macrophage activation trajectories by Vγ4 T cells during skin wound healing

Wengang Hu,[1,2] Xiaorong Zhang,[1,2] Zhongyang Liu,[3] Jiacai Yang,[1,2] Hao Sheng,[4] Zhihui Liu,[1,2] Cheng Chen,[1,2] Ruoyu Shang,[1,2] Yunxia Chen,[1,2] Yifei Lu,[1,2] Xiaohong Hu,[1,2] Yong Huang,[1,2] Wenjing Yin,[5] Xin Cai,[1,2] Dejiang Fan,[1,2] Lingfeng Yan,[1,2] Jianlei Hao,[6,7] Gaoxing Luo,[1,2,8,*] and Weifeng He[1,2,8,9,*]

SUMMARY

Dysregulated macrophage polarization from pro-inflammatory M1 to anti-inflammatory M2 phenotypes underlies impaired cutaneous wound healing. This study reveals Vγ4$^+$ γδ T cells spatiotemporally calibrate macrophage trajectories during skin repair via sophisticated interferon-γ (IFN-γ) conditioning across multiple interconnected tissues. Locally within wound beds, infiltrating Vγ4$^+$ γδ T cells directly potentiate M1 activation and suppress M2 polarization thereby prolonging local inflammation. In draining lymph nodes, infiltrated Vγ4$^+$ γδ T cells expand populations of IFN-γ-competent lymphocytes which disseminate systemically and infiltrate into wound tissues, further enforcing M1 macrophages programming. Moreover, Vγ4$^+$γδ T cells flushed into bone marrow stimulate increased IFN-γ production, which elevates the output of pro-inflammatory Ly6C$^+$monocytes. Mobilization of these monocytes continually replenishes the M1 macrophage pool in wounds, preventing phenotypic conversion to M2 activation. Thus, multi-axis coordination of macrophage activation trajectories by trafficking Vγ4$^+$ γδ T cells provides a sophisticated immunological mechanism regulating inflammation timing and resolution during skin repair.

INTRODUCTION

Efficient cutaneous wound healing is a complex physiological process involving dynamic transitions between overlapping inflammatory, proliferative, and remodeling phases.[1] A hallmark of normal repair is the transient nature of the initial inflammatory response, which is rapidly initiated but timely resolved once its role has been served.[2] However, sustained inflammation represents a major underlying factor contributing to impaired healing outcomes in various chronic wounds and fibrotic disorders.[3–5] Hence, an intricate understanding of the endogenous cellular and molecular pathways governing the cutaneous inflammatory response during tissue repair is imperative.

Of the various immune cells participating in the inflammatory phase, macrophages represent the most abundant and functionally diverse leukocyte population in the dynamic wound microenvironment.[6–8] The changing composition and activation states of heterogeneous macrophage subpopulations are known to be pivotal determinants of tissue healing trajectories and outcomes.[9–11] In the early stage of wound healing, classically activated M1 macrophages accumulate and predominate. They mount strong pro-inflammatory responses integral to host defense, debris clearance, and secretion of factors that initiate the proliferation phase.[12,13] Subsequently, as healing progresses, alternatively activated M2 macrophages accumulate and become dominant within the wound milieu. M2 macrophages potently dampen inflammation while promoting extracellular matrix (ECM) deposition and tissue remodeling.[1,14] This dynamic shift from M1 to M2 phenotypic states provides a necessary immunological switch that curbs inflammation and enables the transition to the later regenerative stages of healing.[15] However, dysregulated macrophage polarization has been increasingly identified as a key pathological feature underlying many chronic non-healing wounds.[6,9,16] Despite these emerging insights, major knowledge gaps remain regarding the intricate endogenous mechanisms that regulate macrophage activation state transitions to control the timing, intensity, and resolution of inflammation during cutaneous repair.

[1]State Key Laboratory of Trauma and Chemical Poisoning, Institute of Burn Research, Southwest Hospital, Third Military Medical University (Army Medical University), Chongqing 400038, China
[2]Chongqing Key Laboratory for Disease Proteomics, Chongqing 400038, China
[3]Department of Plastic Surgery, the First Affiliated Hospital, Zhengzhou University, Henan, China
[4]Urology Department, the Second Affiliated Hospital, Third Military Medical University (Army Medical University), Chongqing 400037, China
[5]Academy of Biological Engineering, Chongqing University, Chongqing, China
[6]Zhuhai Institute of Translational Medicine, Zhuhai People's Hospital Affiliated with Jinan University, Jinan University, Zhuhai 519000 Guangdong, China
[7]The Biomedical Translational Research Institute, Faculty of Medical Science, Jinan University, Guangzhou 510632, Guangdong, China
[8]These authors contributed equally
[9]Lead contact
*Correspondence: logxw@yahoo.com (G.L.), heweifeng@tmmu.edu.cn (W.H.)
https://doi.org/10.1016/j.isci.2024.109545

Recently, T lymphocytes have been recognized as critical early-responding immunomodulators of tissue inflammation and repair in multiple organs.[17–19] Among T cells, γδ T cells comprise an unconventional subset bearing a distinct T cell receptor distinguished by their γ and δ chain usage.[20–22] Although they represent only a minor fraction of circulating T cells, γδ T cells exhibit unique attributes that poise them to be influential regulators of early tissue inflammatory events. These include their abundance in barrier tissues, lack of major histocompatibility complex restrictions, and their ability to rapidly produce copious cytokines upon activation.[23–26] Emerging evidence points to the dynamic involvement of γδ T cell subsets during normal and impaired repair processes in diverse tissues including skin, muscle, bone, cornea, and liver.[18,27,28]

Among the various γδ T cell subsets, Vγ4$^+$ γδ T cells, as the main circulating and residential subset, appear to exhibit specialized wound-homing and immunomodulatory properties.[29,30] In both rodents and humans, Vγ4$^+$ γδ T cells (Vδ2 subset in humans) rapidly accumulate in injured tissues, where they sculpt local inflammatory responses.[31,32] Their wound recruitment and activation are dependent on injury-induced upregulation of Vγ4$^+$ T cell receptor ligands.[33] Once within damaged tissue, Vγ4$^+$ γδ T cells potently produce inflammatory mediators like interleukin-17 (IL-17) and interferon-gamma (IFN-γ), and direct the functions of macrophages, innate lymphoid cells (ILCs) and αβ T cells.[26,34–37] Interestingly, γδ T cell frequencies remain abnormally elevated in chronic wounds compared to acute wounds in murine models and human patients.[17,38,39] Despite these emerging roles in modulating tissue inflammation, the functional impact and mechanisms of action of Vγ4$^+$ γδ T cells during cutaneous wound healing remain obscure.

Some clues are provided by studies demonstrating accelerated wound closure following Vγ4$^+$ γδ T cell depletion in mice.[25] This positions Vγ4$^+$ γδ T cells as putative controllers of the healing program, plausibly through regulation of macrophage activity and polarization.[34] Elucidating the underlying mechanisms will provide seminal insights into γδ T cell-macrophage crosstalk pathways governing inflammation during tissue repair. Defining whether and how Vγ4$^+$ γδ T cells dictate macrophage activation trajectories could unveil novel druggable immunological nodes for therapeutic manipulation in difficult-to-heal wounds.

In this study, we addressed these critical questions by interrogating the functional impact and mechanisms of action of Vγ4$^+$ γδ T cells on macrophage activation phenotypes during cutaneous wound healing. Utilizing murine models coupled with cellular and molecular approaches, we revealed multi-tiered mechanisms by which Vγ4$^+$ γδ T cells orchestrated macrophage polarization over space and time through sophisticated IFN-γ conditioning across tissues. The findings elucidated an intricate innate lymphocyte-myeloid cell signaling circuit controlling the timing, intensity, and resolution of inflammation during skin repair.

RESULTS

Vγ4$^+$ γδ T cells prolong inflammation and delay wound closure

We began by investigating the role of Vγ4$^+$ γδ T cells in modulating the skin wound healing process. Antibody-mediated depletion of Vγ4$^+$ γδ T cells in wild-type mice, which was confirmed by flow cytometry, and the deletion effect of Vγ4 T cells lasted more than 6 weeks at least, which absolutely covered the experimental period, while the injection of isotype antibody didn't deplete Vγ4 T cells (Figure S1A). Depletion of Vγ4 T cells led to markedly expedited wound closure kinetics compared to control mice (Figure 1A). Furthermore, reinstating Vγ4$^+$ γδ T cells into the wound sites of depleted mice reverted the pace of repair back to the slower timeline seen in controls (Figure 1A). This reveals that Vγ4$^+$ γδ T cells inherently delay the healing process. To elucidate the mechanism underlying this delay, we analyzed the expression of pro- and anti-inflammatory cytokines in the wounds. Strikingly, the prototypical pro-inflammatory mediators TNF-α and IL-6 were profoundly suppressed in the wound tissues of Vγ4$^+$ γδ T cell-depleted mice compared to controls, as assessed by immunoblotting and immunohistochemistry (Figures 1B, S1B, and S1C). Moreover, this difference was more pronounced at day 4 versus day 2 post-injury, indicating a specific role of Vγ4$^+$ γδ T cells in prolonging inflammation over time. Conversely, the anti-inflammatory factors TGF-β and IL-10 were markedly upregulated in the wounds of Vγ4$^+$ γδ T cell-depleted mice (Figures S1C–S1E), implying an accelerated resolution of inflammation without these cells. Again, the extent of the increase was greater on day 4 compared to day 2. Strikingly, re-introducing Vγ4$^+$ γδ T cells into depleted mice restored high TNF-α/IL-6 and low TGF-β/IL-10 expression patterns that delayed inflammation termination (Figures 1B, 1C, and S1B–S1E).

Together, these compelling results reveal that Vγ4$^+$ γδ T cells are indispensable controllers of inflammation duration during skin repair, prolonging the early inflammatory phase while suppressing timely resolution.

Vγ4$^+$ γδ T cells impede the macrophage phenotypic switch from M1 to M2

We next investigated whether Vγ4$^+$ γδ T cells regulate inflammation by modulating macrophage polarization dynamics. Flow cytometry demonstrated that overall CD11b$^+$ myeloid cell infiltration into wound sites was unaltered upon Vγ4$^+$ γδ T cell depletion (Figure S1F). However, the composition of myeloid cells was markedly changed. On day 2 post-injury, the frequency of proinflammatory Ly6G$^+$ neutrophils among CD11b$^+$ cells was unchanged (Figure 2A). Strikingly, by day 4, Ly6G$^+$ neutrophil percentages were significantly reduced without Vγ4$^+$ γδ T cells (Figure 2A), indicating accelerated conversion to a monocyte/macrophage-dominant state. We then examined the proportion of M1 among all macrophages, the markers F4/80 in combination with CD11b were usually applied to mark macrophages,[40,41] however, it was found >95% of F4/80$^+$ cells were CD11b$^+$ in the wound samples of day 2 and day 4 (Figure S2), so the sole marker F4/80 was chosen to distinguish macrophages as some papers did.[42,43] On day 2, M1 percentages were similar between Vγ4$^+$ γδ T cell depleted and control mice, based on flow cytometric and immunofluorescent analysis of the M1 markers CD86 and iNOS (Figures 2B and 2C). However, by day 4, the M1 fraction was profoundly reduced without Vγ4$^+$ γδ T cells (Figures 2B and 2C). This M1 decline was substantiated by decreased mRNA expression of the M1-associated molecules iNOS and TNF-α (Figures 2D and 2E). Remarkably, transferring Vγ4$^+$ γδ T cells into depleted mice restored high M1 percentages and M1 factor expression on day 4 (Figures 2B–2E). Assessing M2 macrophage dynamics revealed a reciprocal increase by day 4

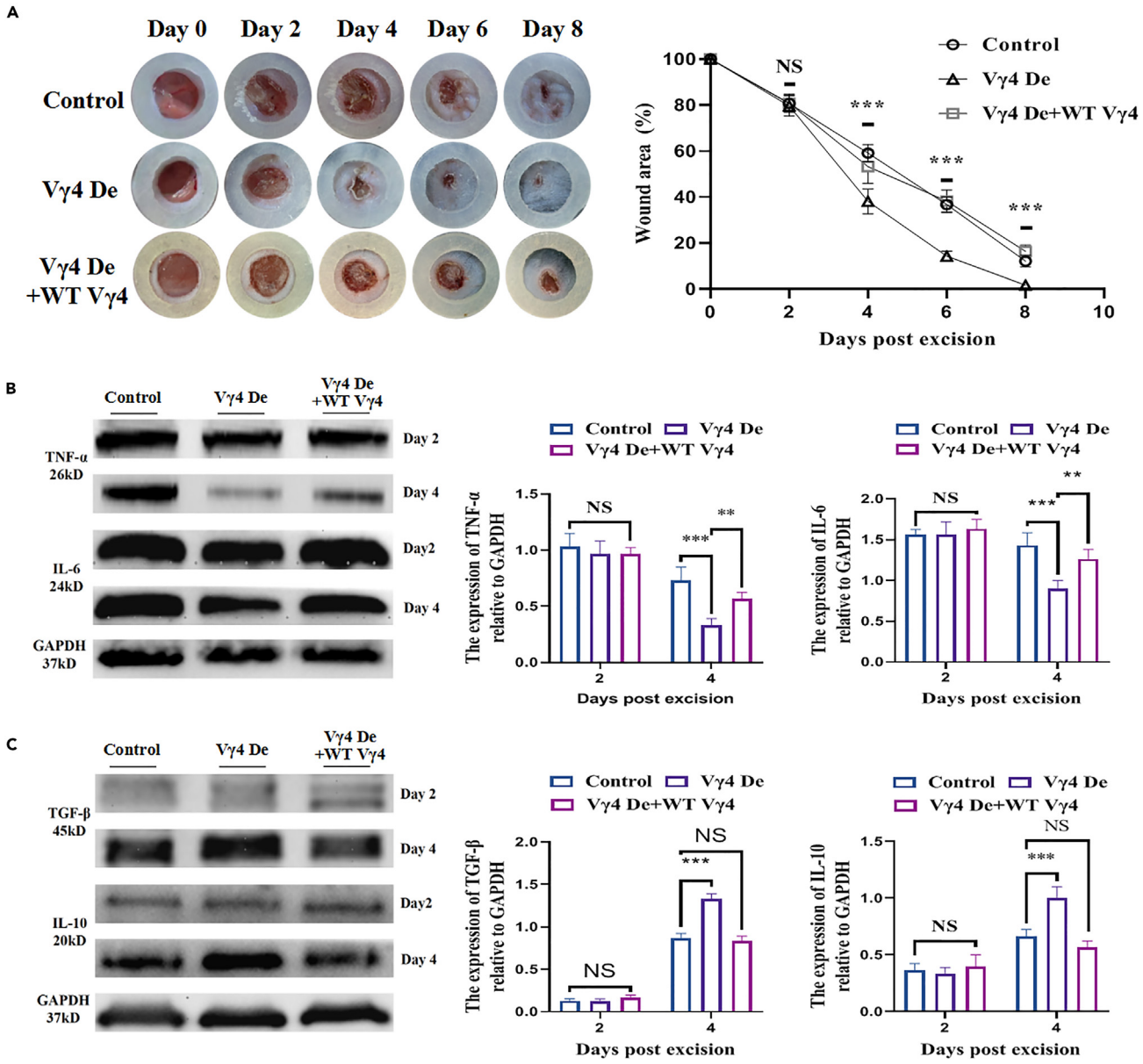

Figure 1. Vγ4 T cells prolong inflammation contributing to delayed skin wound healing

(A) Wound-closure kinetics of three groups. Group 1: Control (WT + Isotype); group 2: Vγ4 Depleted (Vγ4 De); group 3: Vγ4 De+WT Vγ4 T cells (wound-derived Vγ4 T cells cultured for 7 days were locally injected into the skin around the wound edge, 5×10^5/wound). Mice of different groups were age, sex and weight-matched. Wound area (%) was measured to analyze the wound-closure kinetics, n = 10 (2 wounds/mouse, 5 mice/group).

(B) Pro-inflammatory cytokines TNFα and IL-6 production analysis of wound lysates on 2nd and 4th days post-injury in Control, Vγ4 De and Vγ4 De+WT Vγ4 mice by means of western blot (WB). (n = 3 mice per group per time point, compiled from two independent experiments).

(C) Anti-inflammatory cytokines TGF-β and IL-10 production analysis of wound lysates on indicated days in Control, Vγ4 De and Vγ4 De+WT Vγ4 mice by WB (n = 3 mice). Bars show the Mean ± SD. One-way ANOVA with Tukey's multiple comparisons test was applied to calculate the p value. *, $p < 0.05$; **, $p < 0.01$; ***, $p < 0.001$; NS, not significant.

without Vγ4$^+$ γδ T cells, evidenced by elevated frequencies of CD206$^+$ and Arg1$^+$ M2 macrophages and increased Arg-1 and Ym1 expression (Figures 2F–2I). Vγ4$^+$ γδ T cell transfer prevented this rise (Figures 2F–2I). To exclude the influence on macrophage polarization caused by isotype antibody, the M1 or M2 proportion in macrophages of WT and control group (WT + Isotype antibody) was analyzed, the results indicated that the macrophages of the two groups showed identical polarizing trends on the 2nd and 4th days (Figures S3A and S3B), the failed depletion of Vγ4 T cells didn't influence the wound healing efficiency (Figures S3C–S3E).

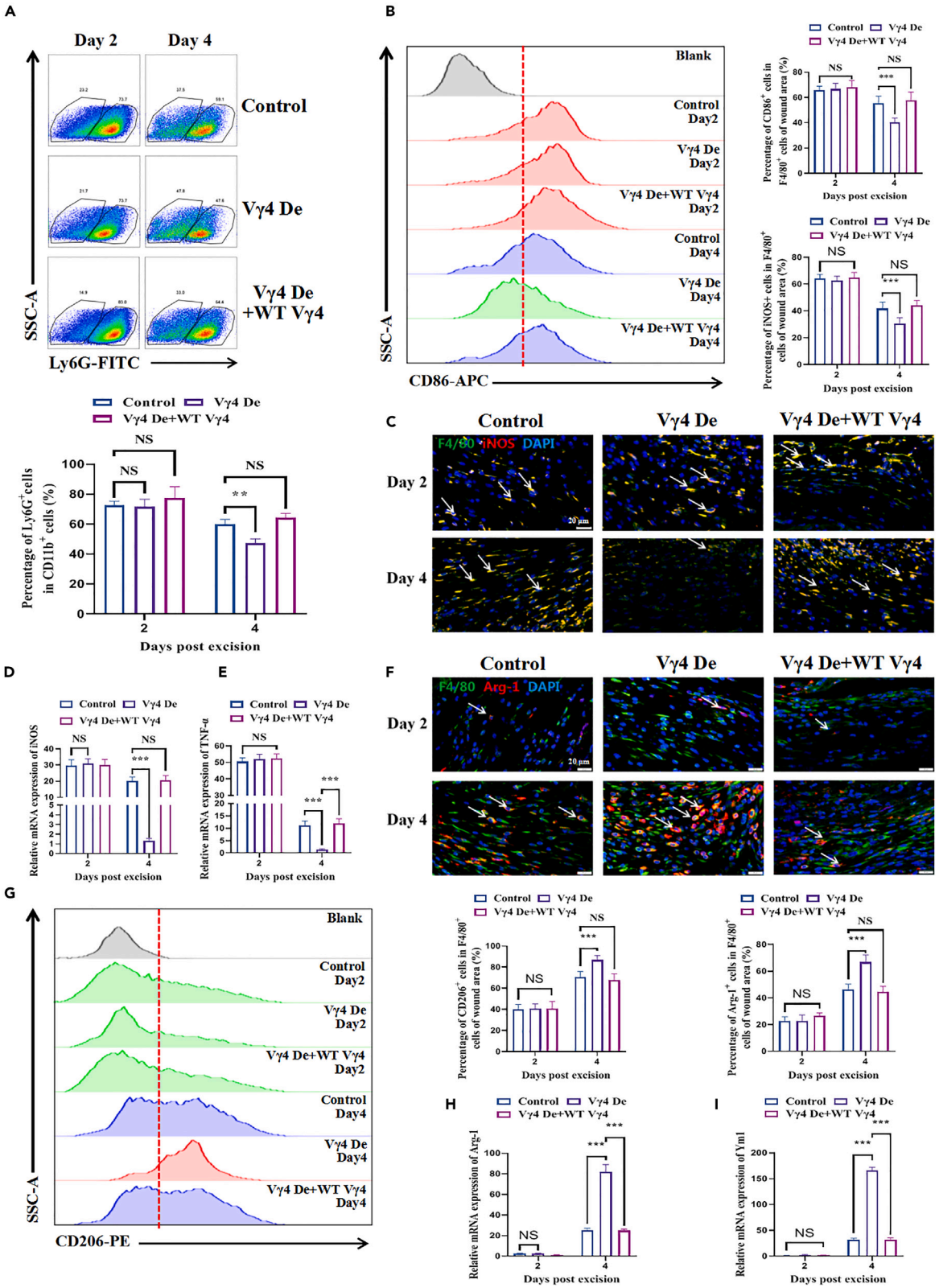
A
Day 2
Day 4
Control
Vγ4 De
Vγ4 De +WT Vγ4
SSC-A
Ly6G-FITC
B
Blank
Control Day2
Vγ4 De Day2
Vγ4 De+WT Vγ4 Day2
Control Day4
Vγ4 De Day4
Vγ4 De+WT Vγ4 Day4
SSC-A
CD86-APC
Control
Vγ4 De
Vγ4 De+WT Vγ4
Percentage of CD86+ cells in F4/80+ cells of wound area (%)
Percentage of iNOS+ cells in F4/80+ cells of wound area (%)
Days post excision
NS
***
Control
Vγ4 De
Vγ4 De+WT Vγ4
Percentage of Ly6G+ cells in CD11b+ cells (%)
Days post excision
NS
**
C
Control
Vγ4 De
Vγ4 De+WT Vγ4
Day 2
Day 4
F4/80 iNOS DAPI
20 μm
D
Relative mRNA expression of iNOS
Days post excision
E
Relative mRNA expression of TNF-α
Days post excision
F
Control
Vγ4 De
Vγ4 De+WT Vγ4
Day 2
Day 4
F4/80 Arg-1 DAPI
20 μm
G
Blank
Control Day2
Vγ4 De Day2
Vγ4 De+WT Vγ4 Day2
Control Day4
Vγ4 De Day4
Vγ4 De+WT Vγ4 Day4
SSC-A
CD206-PE
Percentage of CD206+ cells in F4/80+ cells of wound area (%)
Days post excision
Percentage of Arg-1+ cells in F4/80+ cells of wound area (%)
Days post excision
H
Relative mRNA expression of Arg-1
Days post excision
I
Relative mRNA expression of Ym1
Days post excision

Figure 2. Vγ4 T cells impede macrophage phenotype conversion from M1 to M2

(A) Flow cytometry quantifying Ly6G$^+$ neutrophil frequency among CD11b$^+$ cells in wound digests on the 2nd and 4th days post-injury in Control, Vγ4 De and Vγ4 De+WT Vγ4 mice (n = 4 mice per group).

(B) Flow cytometry quantifying CD86$^+$ M1 macrophage frequency among F4/80$^+$ cells in wound digests on indicated days (n = 4 mice per group).

(C) Immunofluorescence staining and quantification of iNOS$^+$ M1 macrophages in wound sections on indicated days (n = 4 mice per group), scale bar, 20 μm.

(D) Quantitative PCR (qPCR) analysis of iNOS mRNA expression in wound lysates on indicated days (n = 4 mice per group).

(E) qPCR analysis of TNFα mRNA expression in wound lysates on indicated days (n = 4 mice per group).

(F) Immunofluorescence staining and quantification of Arg1$^+$ M2 macrophages in wound sections on indicated days (n = 4 mice per group), scale bar, 20 μm.

(G) Flow cytometry quantifying CD206$^+$ M2 macrophage frequency among F4/80$^+$ cells in wound digests on indicated days (n = 4 mice per group).

(H) qPCR analysis of Arg-1 mRNA expression in wound lysates on indicated days (n = 4 mice per group).

(I) qPCR analysis of Ym1 mRNA expression in wound lysates on indicated days (n = 4 mice per group). Bars show the Mean ± SD. One-way ANOVA with Tukey's multiple comparisons test was applied to calculate the p value. *, $p < 0.05$; **, $p < 0.01$; ***, $p < 0.001$; NS, not significant. The arrows in the figures indicate the positive staining.

Together, these compelling data strongly suggest Vγ4$^+$ γδ T cells potently delay the macrophage phenotypic switch from inflammatory M1 to anti-inflammatory M2 activation states during skin healing.

Vγ4+ γδ T cells directly interact with macrophages to skew M1 polarization

We next evaluated whether Vγ4$^+$ γδ T cells directly interface with macrophages by co-localizing the two cell types in wound tissues on the 4th day post-injury using confocal microscopy. Strikingly, overt co-localization of Vγ4$^+$ γδ T cells with macrophages was readily observed within wound beds (Figure 3A). Similar results were obtained from the analysis of implanted sponges (Figures S4A and S4B). To further dissect the functional impact of these interactions on macrophage polarization, we utilized an *in vitro* co-culture system. Vγ4$^+$ γδ T cells (their purity was >95%, Figures S4C and S4D) profoundly enhanced M1 activation of bone marrow-derived macrophages (BMDMs) (their purity was >95%, Figures S4E and S4F), dramatically increasing the percentages of CD86$^+$ and iNOS$^+$ M1 macrophages (Figures 3B, 3C, S4G, and S4H) and expression of TNF-α and IL-6 (Figures 3D, 3E, S4I, and S4J) upon LPS (Lipopolysaccharide) stimulation. Conversely, Vγ4$^+$ γδ T cells potently suppressed IL-4-induced M2 activation, markedly reducing CD206$^+$ and Arg1$^+$ macrophage frequencies (Figures 3F, 3G, S4K, and S4L) and TGF-β/IL-10 production (Figures 3H, 3I, S4M, and S4N). Strikingly, Vγ4$^+$ γδ T cells also strongly inhibited M1-to-M2 phenotypic conversion (Figures 3J–3M and S4O–S4R).

Collectively, these functional experiments directly demonstrate that Vγ4$^+$ γδ T cells interface with macrophages and skew their polarization toward sustained proinflammatory M1 activation while restricting anti-inflammatory M2 phenotypes. This ability to modulate macrophage immunometabolism likely enables Vγ4$^+$ γδ T cells to calibrate inflammatory responses during skin repair.

Vγ4$^+$ γδ T cell-driven macrophage polarization depends on IFN-γ

We next sought to define the molecular factors mediating the modulatory effects of Vγ4$^+$ γδ T cells on macrophage activation trajectories. Transwell experiment discovered the effect of Vγ4 T cells in promoting iNOS expression was significantly attenuated when co-cultured with macrophages separately, confirming that the non-cellular contact was the main regulating approach (Figure S5A). ELISA revealed markedly higher IFN-γ levels in Vγ4$^+$ γδ T cell-macrophage co-cultures versus macrophage alone cultures (Figure 4A). Flow cytometry demonstrated that Vγ4$^+$ γδ T cells secreted plenty of IFN-γ (Figure 4B). Neutralizing IFN-γ or utilizing IFN-γ-deficient Vγ4$^+$ γδ T cells almost entirely mitigated the ability of wild-type Vγ4$^+$ γδ T cells in enhancing M1 activation, evidenced by impaired upregulation of CD86, iNOS, TNF-α, and IL-6 (Figures 4C–4E, S5B, and S5C). Similarly, IFN-γ neutralization or deficiency abrogated the M2-inhibitory effects, as shown by restored CD206, Arg1, TGF-β, and IL-10 expression (Figures 4F–4H, S5D, and S5E). IFN-γ ablation also relieved the suppression of M1-to-M2 conversion (Figures 4I, 4J, S5F, and S5G). The effectiveness of the IFN-γ gene knockout was verified through IFN-γ-specific flow cytometry, Vγ4 T cells cultured from IFN-γ$^{-/-}$ mice were almost incapable of secreting IFN-γ in comparison with those from wilder type mice (Figure S6).

These functional experiments identify IFN-γ as the critical factor underlying Vγ4$^+$ γδ T cell orchestration of macrophage activation trajectories during skin wound healing.

IFNγ production by Vγ4$^+$ γδ T cells is required to modulate macrophages skewing and delay wound healing

Although our data indicated a key role for Vγ4$^+$ γδ T cell-derived IFN-γ in impeding M1-to-M2 switching, whether IFN-γ secretion was indispensable for their ability to delay skin repair remained to be established. Strikingly, transferring IFN-γ-competent but not IFN-γ-deficient Vγ4$^+$ γδ T cells into Vγ4$^+$ γδ T cell-depleted mice substantially delayed wound closure kinetics, accompanied by delayed granulation tissue formation and slow epithelial tongue advancement (Figures 5A and S7A). IFN-γ-deficient Vγ4$^+$ γδ T cells also failed to sustain high M1 marker expression in wound macrophages by day 4 (Figures 5B and 5C). Moreover, they were impaired in suppressing M2 marker upregulation compared to wild-type Vγ4$^+$ γδ T cells (Figures 5D–5G). Finally, only IFN-γ-sufficient Vγ4$^+$ γδ T cells restored the diminished frequencies of total IFN-γ-producing cells and levels of IFN-γ in the wounds of Vγ4$^+$ γδ T cell-depleted mice (Figure 5H).

Together, these *in vivo* experiments definitively demonstrate that IFN-γ production specifically by Vγ4$^+$ γδ T cells is indispensable for their ability to delay cutaneous wound closure and macrophage phenotype switching from inflammatory M1 to anti-inflammatory M2 activation state during skin repair.

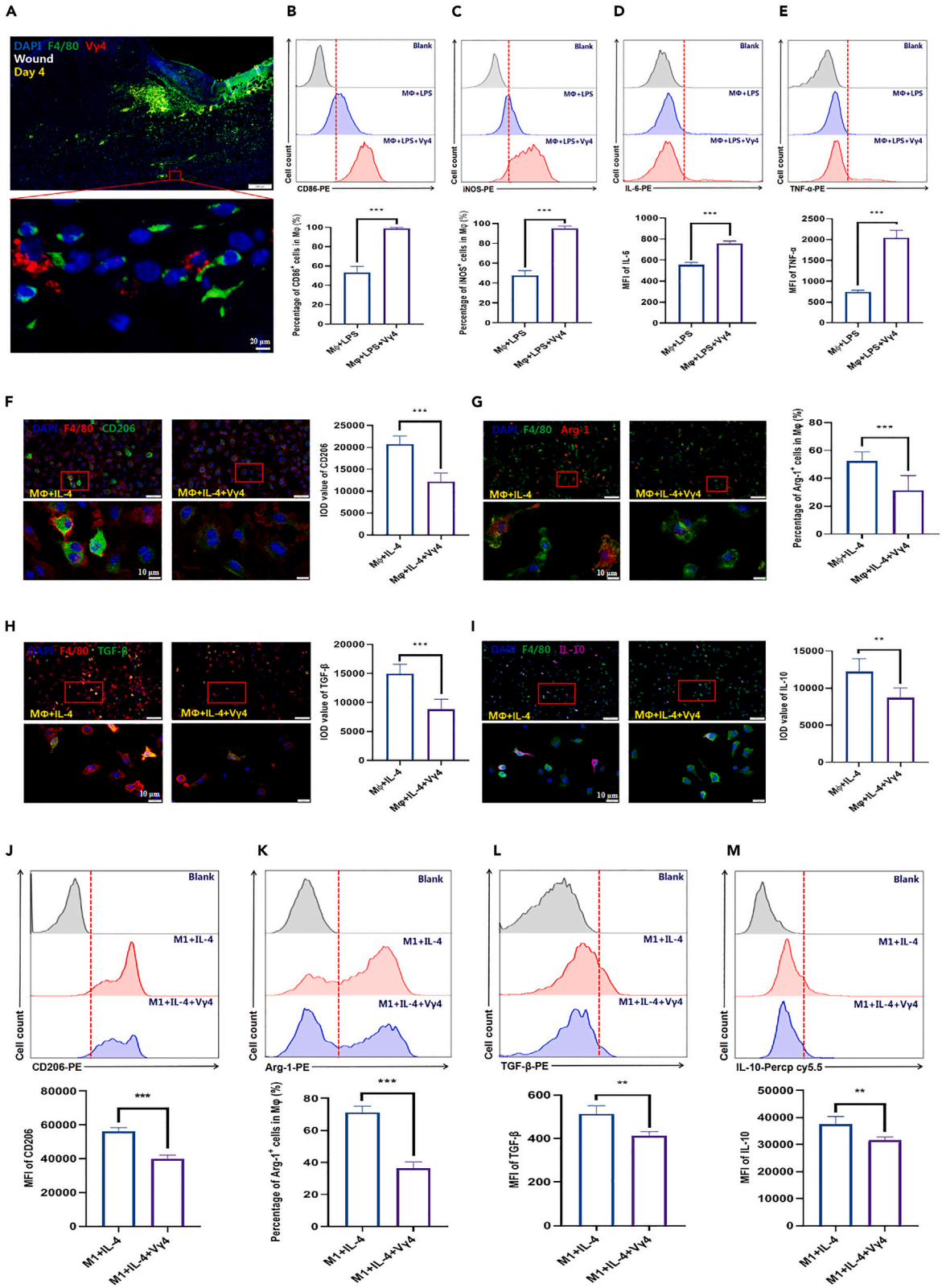
A
DAPI F4/80 Vγ4
Wound
Day 4
20 μm
B
Blank
MΦ+LPS
MΦ+LPS+Vγ4
Cell count
CD86-PE
Percentage of CD86+ cells in Mφ (%)
MΦ+LPS
MΦ+LPS+Vγ4
C
Blank
MΦ+LPS
MΦ+LPS+Vγ4
Cell count
iNOS-PE
Percentage of iNOS+ cells in Mφ (%)
MΦ+LPS
MΦ+LPS+Vγ4
D
Blank
MΦ+LPS
MΦ+LPS+Vγ4
Cell count
IL-6-PE
MFI of IL-6
MΦ+LPS
MΦ+LPS+Vγ4
E
Blank
MΦ+LPS
MΦ+LPS+Vγ4
Cell count
TNF-α-PE
MFI of TNF-α
MΦ+LPS
MΦ+LPS+Vγ4
F
DAPI F4/80 CD206
MΦ+IL-4
MΦ+IL-4+Vγ4
10 μm
IOD value of CD206
MΦ+IL-4
MΦ+IL-4+Vγ4
G
DAPI F4/80 Arg-1
MΦ+IL-4
MΦ+IL-4+Vγ4
10 μm
Percentage of Arg-1+ cells in Mφ (%)
MΦ+IL-4
MΦ+IL-4+Vγ4
H
DAPI F4/80 TGF-β
MΦ+IL-4
MΦ+IL-4+Vγ4
10 μm
IOD value of TGF-β
MΦ+IL-4
MΦ+IL-4+Vγ4
I
DAPI F4/80 IL-10
MΦ+IL-4
MΦ+IL-4+Vγ4
10 μm
IOD value of IL-10
MΦ+IL-4
MΦ+IL-4+Vγ4
J
Blank
M1+IL-4
M1+IL-4+Vγ4
Cell count
CD206-PE
MFI of CD206
M1+IL-4
M1+IL-4+Vγ4
K
Blank
M1+IL-4
M1+IL-4+Vγ4
Cell count
Arg-1-PE
Percentage of Arg-1+ cells in Mφ (%)
M1+IL-4
M1+IL-4+Vγ4
L
Blank
M1+IL-4
M1+IL-4+Vγ4
Cell count
TGF-β-PE
MFI of TGF-β
M1+IL-4
M1+IL-4+Vγ4
M
Blank
M1+IL-4
M1+IL-4+Vγ4
Cell count
IL-10-Percp cy5.5
MFI of IL-10
M1+IL-4
M1+IL-4+Vγ4

Figure 3. Vγ4+ γδ T cells directly interact with macrophages to skew M1 polarization and impede M2 polarization

(A) Confocal microscopy visualizing Vγ4 T cells (red) interacting with F4/80$^+$ macrophages (green) in wounded skin on the 4^{the} day post-injury. Nuclei stained with DAPI (blue). Representative of three independent experiments, scale bar, 20 μm.

(B–E) Flow cytometry quantifying CD86, iNOS, IL-6 and TNFα expression among LPS-stimulated bone marrow-derived macrophages (BMDMs) after culturing alone or with Vγ4 T cells (n = 4 per group, compiled from two independent experiments).

(F–I) Immunofluorescence staining quantifying CD206, Arg-1, TGF-β and IL-10 expression among IL-4 stimulated BMDMs of the indicated two groups, respectively, scale bar, 10 μm, n = 5 per group, compiled from two independent experiments.

(J–M) Flow cytometry quantifying CD206, Arg-1, TGF-β, and IL-10 expression among IL-4 stimulated M1 macrophages after culturing alone or with Vγ4 T cells (n = 4 per group, compiled from two independent experiments). Bars show the Mean ± SD. Unpaired two-tailed t-test was applied to calculate the p value (B, C, D, E, F, G, H, I, J, K, L, and M). *, $p < 0.05$; **, $p < 0.01$; ***, $p < 0.001$; NS, not significant.

Vγ4$^+$ γδ T cells license IFN-γ$^+$ lymphocytes in multiple tissues

Although important, we found that direct IFN-γ secretion by Vγ4$^+$ γδ T cells only modestly contributed to total wound IFN-γ levels based on intracellular staining (Figure S7B). This implied additional indirect mechanisms of boosting IFN-γ. Notably, approximately 60–70% of IFN-γ+ cells in wounds were CD3$^+$ lymphocytes (Figure 6A). We postulated that Vγ4$^+$ γδ T cells may license other IFN-γ-competent CD3$^+$ lymphocytes to propagate inflammatory macrophage programming. Firstly, in draining lymph nodes, IFN-γ$^+$ cell frequencies markedly increased after injury to ~7%, mostly CD3$^+$ cells (Figure 6B). Strikingly, this expansion was abrogated by ~50% upon Vγ4$^+$ γδ T cell depletion. Transfer of wild type but not IFN-γ-deficient Vγ4$^+$ γδ T cells into depleted mice rescued the IFN-γ$^+$ cell expansion in lymph node, as well as blood (Figures 6B and 6C). Analogous dynamics occurred systemically. The percentage of circulating IFN-γ$^+$ cells increased after injury to ~8%, predominantly CD3$^+$ lymphocytes, but was reduced to ~6% with Vγ4$^+$ γδ T cell depletion (Figure 6C). Again, wild type but not IFN-γ-deficient Vγ4$^+$ γδ T cell transfer restored high levels (Figure 6C). Secondly, tracking experiments revealed that Vγ4$^+$ γδ T cells transiently infiltrate lymph nodes and wound area, peaking at day 3 before declining by day 7 post-injury (Figures 6D, 6E, S7C, and S7D). This positions them to locally prime IFN-γ$^+$ lymphocytes. Mirroring lymph node and wound area patterns, circulating Vγ4$^+$ γδ T cells showed marked but transient depletion after injury before rebounding (Figures 6F and S7E), indicative of systemic redistribution. Intravenous transfer experiments confirmed infiltration of circulating Vγ4$^+$ γδ T cells into both wounded tissues and lymph nodes (Figures 6G and 6H). In addition, wound area Vγ4$^+$ γδ T cells also flushed into both blood and lymph nodes upon wounding (Figures 6I and 6J).

Collectively, these findings reveal a sophisticated mechanism whereby Vγ4$^+$ γδ T cells orchestrate IFN-γ production across multiple tissues by transiently infiltrating wounds, lymph nodes, and circulation to license IFN-γ$^+$ lymphocytes. These expanded IFN-γ$^+$ lymphocytes persist and provide enduring IFN-γ signals that shape macrophage activation trajectories throughout healing.

Vγ4$^+$ γδ T cells remotely program monocyte generation via bone marrow IFN-γ conditioning

Finally, we elucidated an unexpected remote signaling axis by which Vγ4$^+$ γδ T cells coordinate macrophage responses between the bone marrow and wound sites. Tracking experiments revealed transient infiltration of the bone marrow by Vγ4$^+$ γδ T cells after injury, peaking at day 5 (Figures 7A–7C and S7F). This coincided with increased frequencies of bone marrow IFN-γ$^+$ cells (Figure 7D). Strikingly, bone marrow IFN-γ$^+$ cell accumulation was almost entirely ablated by Vγ4$^+$ γδ T cell depletion but rescued by wild-type Vγ4$^+$ γδ T cell transfer (Figure 7D).

Functionally, depletion of Vγ4$^+$ γδ T cells led to reduced output of pro-inflammatory Ly6C$^+$ monocytes from the bone marrow (Figure 7E), correlating with diminished levels in circulation (Figure 7F) and impaired Ly6C$^+$ monocyte wound recruitment (Figure 7G). WT but not IFN-γ-deficient Vγ4$^+$ γδ T cell administration restored high systemic Ly6C$^+$ monocyte levels and wound infiltration (Figures 7E–7G). Mechanistically, Ly6C$^+$ monocyte replenishment prevented the eventual M1-to-M2 macrophage phenotypic switch in wounds by sustaining inflammatory macrophage marker expression (Figures 5B–5E).

These findings elucidate a remote bone marrow-blood-wound signaling axis coordinated by bone marrow infiltration and IFN-γ production of Vγ4$^+$ γδ T cells. Vγ4$^+$ γδ T cell-derived IFN-γ generation in the bone marrow augments the output of pro-inflammatory Ly6C$^+$ monocytes, which migrate to wounds and continually reinforce inflammatory M1 macrophage activation.

DISCUSSION

Cutaneous wound healing is orchestrated by multiple innate and the adaptive immune cells including neutrophils, mast cells, dendritic cells (DCs), T cells, macrophages, and ILCs, among them, each population plays distinct and specific role in wound repair.[44] Neutrophils are capable of phagocytosing and killing contaminated microorganisms, mast cells can help to promote inflammation via helping to attract more immune cells to the wound.[1] DCs are antigen-presenting cells which are generally involved in priming T cell responses.[45] Innate lymphoid cells (ILCs, comprising NK cells, ILC1s, ILC2s, ILC3s, and LTi cells) are newly identified members of the innate immune system,[46,47] IL-33-sensitive ILC2s play a host-protective tissue reparative role in restoring cutaneous barrier functions.[48,49] T cells are able to influence inflammation via modulating other immune cells during wound repair.[19] However, monocytes and macrophages are central regulators of healing, with dynamic transitions from pro-inflammatory M1 to anti-inflammatory M2 activation states being indispensable for efficient repair.[10,50,51] This study elucidates multi-tiered mechanisms by which Vγ4$^+$ γδ T cells calibrate macrophage activation phenotypes during skin repair through sophisticated IFN-γ conditioning.

Locally within injured skin, we found that circulating Vγ4$^+$ γδ T cells are capable of migrating into the wound area after intravenous injection, same as the migration into wounded liver, brain, and spinal cord.[26,52,53] CCR6 and CCR2 were recognized to be involved in this

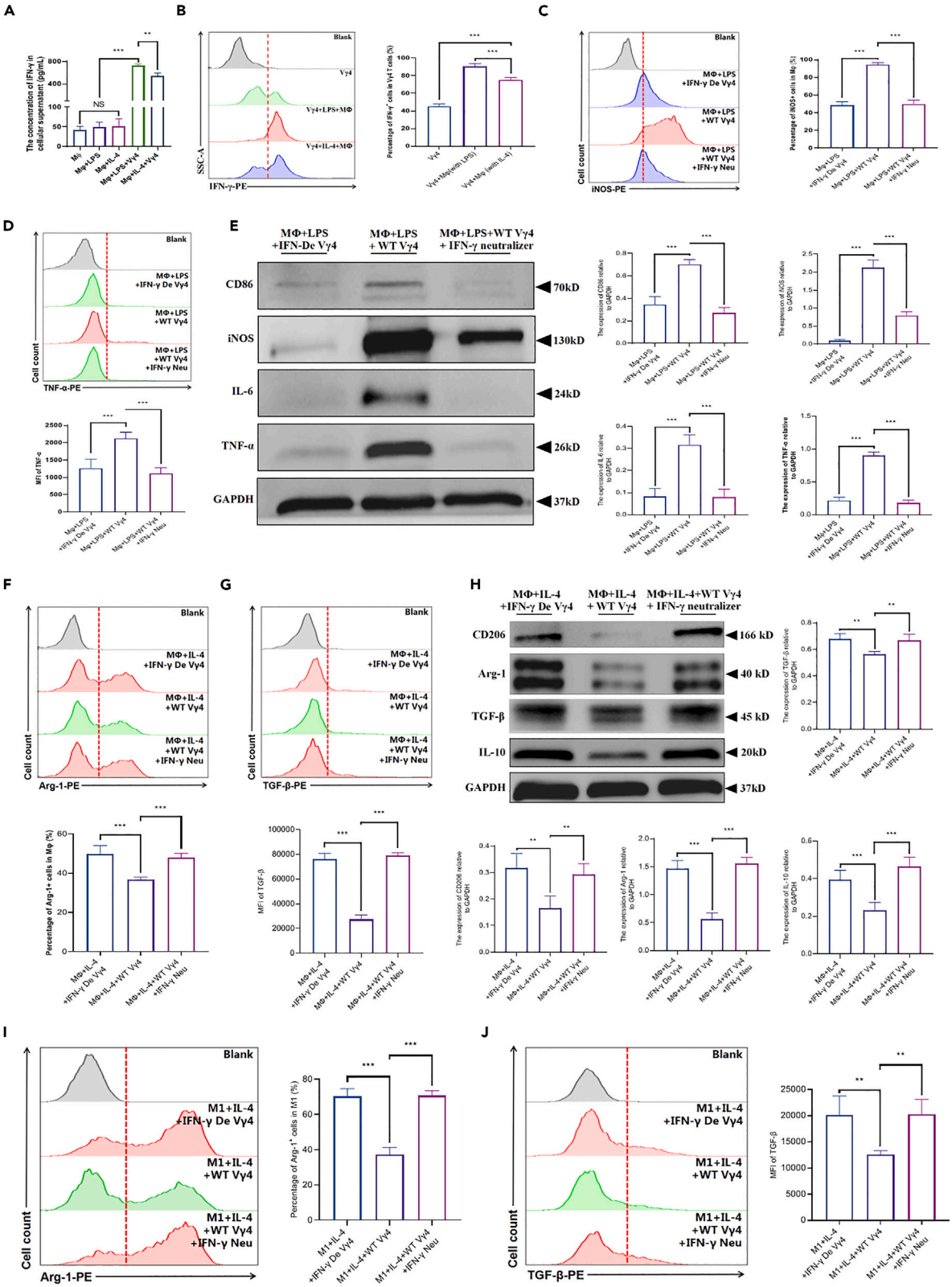
A
B
C
D
E
F
G
H
I
J
Blank
Vγ4
Vγ4+LPS+MΦ
Vγ4+IL-4+MΦ
MΦ+LPS +IFN-γ De Vγ4
MΦ+LPS +WT Vγ4
MΦ+LPS +WT Vγ4 +IFN-γ Neu
MΦ+LPS +IFN-De Vγ4
MΦ+LPS + WT Vγ4
MΦ+LPS+WT Vγ4 + IFN-γ neutralizer
CD86
iNOS
IL-6
TNF-α
GAPDH
70kD
130kD
24kD
26kD
37kD
MΦ+IL-4 +IFN-γ De Vγ4
MΦ+IL-4 + WT Vγ4
MΦ+IL-4+WT Vγ4 + IFN-γ neutralizer
CD206
Arg-1
TGF-β
IL-10
166 kD
40 kD
45 kD
20kD
M1+IL-4 +IFN-γ De Vγ4
M1+IL-4 +WT Vγ4
M1+IL-4 +WT Vγ4 +IFN-γ Neu
Cell count
TNF-α-PE
Arg-1-PE
TGF-β-PE
iNOS-PE
SSC-A
IFN-γ-PE

Figure 4. Vγ4 T cells modulate macrophage polarization via IFN-γ secretion

(A) ELISA quantifying IFN-γ concentration in culture supernatants of BMDMs cultured alone or with Vγ4 T cells, with LPS or IL-4 stimulation (n = 4 per group, compiled from two independent experiments).

(B) Flow cytometry quantifying IFN-γ^+ frequency among Vγ4 T cells cultured alone or with BMDMs, under LPS or IL-4 stimulation (n = 4 per group, compiled from two independent experiments).

(C and D) Flow cytometry quantifying iNOS$^+$ frequency and mean fluorescence intensity (MFI) of TNF-α expression among LPS-stimulated BMDMs of the three groups (Cultured with IFN-γ Deficient Vγ4 T cells, with WT Vγ4 T cells, and with WT Vγ4 T cells coupled with IFN-γ neutralizing antibody), n = 4 replicates per group compiled from two independent experiments.

(E) Western blot analysis of CD86, iNOS, TNFα, and IL-6 expression in LPS-stimulated BMDMs of the indicated three groups, n = 3 replicates per group compiled from two independent experiments.

(F and G) Flow cytometry quantifying Arg1$^+$ frequency and the MFI of TGF-β expression among IL-4-stimulated BMDMs of the indicated three groups, n = 4 replicates per group compiled from two independent experiments.

(H) Western blot analysis of CD206, Arg1, TGFβ, and IL-10 expression in IL-4-stimulated BMDMs of the indicated three groups, n = 3 replicates per group compiled from two independent experiments.

(I and J) Flow cytometry quantifying Arg1$^+$ frequency and the MFI of TGF-β expression among IL-4 stimulated M1 of the indicated three groups, n = 4 replicates per group compiled from two independent experiments. Bars show the Mean ± SD. One-way ANOVA with Tukey's multiple comparisons test was applied to calculate the p value. *, $p < 0.05$; **, $p < 0.01$; ***, $p < 0.001$; NS, not significant.

migration,[53–55] whether they are important molecules in driving Vγ4 T cells into skin wounds is indeterminate. Increased Vγ4 T cells facilitated the pro-inflammatory environment packed with many neutrophils, and sustained inflammatory M1 macrophage responses while restricting the accumulation of wound-resolving M2 macrophages, which delayed the termination of inflammation,[56] thereby transiently hindering wound closure, and these results were consistent with the findings of γδ T cells up-regulating iNOS expression in a murine scald model.[57–59] Mechanistically, direct Vγ4$^+$ γδ T cell-macrophage interactions within damaged tissue sites skew macrophage polarization toward M1 activation and away from M2 phenotypes in an IFN-γ-dependent manner. This local calibration of macrophage activation trajectories provides an immunological brake that prevents premature resolution of the inflammatory phase before its duties have been adequately fulfilled.[60,61]

Beyond paracrine signaling within wound beds, we reveal multi-organ communication circuits coordinated by Vγ4$^+$ γδ T cell trafficking that further propagate inflammatory macrophage programming. In draining lymph nodes, infiltrating Vγ4$^+$ γδ T cells expand and mobilize IFN-γ-competent lymphocytes into circulation. These cells disseminate systemically and infiltrate into wounds, supplementing local IFN-γ levels to further enforce M1 polarization. Thus, Vγ4$^+$ γδ T cells do not solely modulate macrophages through direct contact, but also engage adaptive lymphocytes to potentiate and disseminate their influence.

Remarkably, we also uncover that Vγ4$^+$ γδ T cells enact long-range control over myeloid cell fates between the bone marrow and wound sites. Transitory bone marrow infiltration stimulates CD3$^-$ bone marrow cells-derived IFN-γ production. Increased IFN-γ is capable of driving increased generation and mobilization of pro-inflammatory Ly6C$^+$ monocytes, which was confirmed by previous studies.[62–64] Continual recruitment of these monocytes to wounds sustains inflammatory macrophage activation by preventing phenotypic conversion to M2.[65–68] This unexpected remote signaling axis expands the sphere of influence of Vγ4$^+$ γδ T cells over macrophage trajectory patterns during skin repair. Actually remote regulation existed in many physiologic and pathologic conditions, catecholamines are remotely secreted into the circulation by the sympathetic nervous system (SNS) and bind to adrenoreceptors expressed on the surface of lymphocytes to affect their trafficking, circulation, proliferation, and cytokine production.[69,70] Under major trauma or injury, overactivation of the SNS usually contributes to suppressed cellular immunity, via an induction of a Th2 shift, which is associated with a higher incidence infection.[71,72] Besides, many leukocytes such as naive and memory T cells, memory B cells, plasma cells are capable of entering into bone marrow.[73] So, modulation of bone marrow precursors by infiltrating Vγ4 T cells has plausible precedence, however, the mechanism of traffic is not explored, but deserves further study.

Conceptually, this work significantly advances understanding of the endogenous immunological pathways governing macrophage activation during tissue healing. One previous study discovered it was Vγ4 T cells capable of secreting IL-17A, not IFN-γ that migrated into epidermis to regulate DETCs, leading to inhibited IGF-1 production and thus delayed wound healing.[25] The present research excavated their role in another aspect, which positions motile Vγ4$^+$ γδ T cells as pivotal early responding rheostats that calibrate the onset, magnitude, and duration of cutaneous inflammation via multi-axis IFN-γ conditioning. The ability to mobilize rapidly from barrier sites allows Vγ4$^+$ γδ T cells to coordinate evolving responses across interconnected tissue microenvironments. Dynamic infiltration enables the calibration of macrophage immunometabolism locally within wounds, systemically through secondary lymphoid organs, and remotely via bone marrow precursors. IFN-γ production is revealed as a defining feature enabling Vγ4$^+$ γδ T cells to modulate macrophage polarization across these anatomical compartments.

The mechanisms delineated here likely operate during regular acute healing to prevent inadequate or mistimed repair due to prematured inflammatory resolution.[74,75] However, persistent dysregulation of this Vγ4$^+$ γδ T cell-macrophage signaling axis may contribute to pathological inflammation and impaired healing in chronic wounds.[76–78] Current findings and emerging human data position Vγ4$^+$ γδ T cells (Vδ2 γδ T cells in human) as drivers of sustained inflammation in chronic wounds through aberrant trafficking, localization, activation, and IFN-γ production.[79,80] Ongoing reinforcement of M1 activation programs by infiltrating Vγ4$^+$ γδ T cells and Ly6C$^+$ monocytes may represent a core pathological feature underlying macrophage dysfunction in non-healing wounds.[81,82] Looking forward, directly assessing the activity patterns and immunomodulatory roles of human γδ T cells in acute versus chronic wound contexts will be informative.

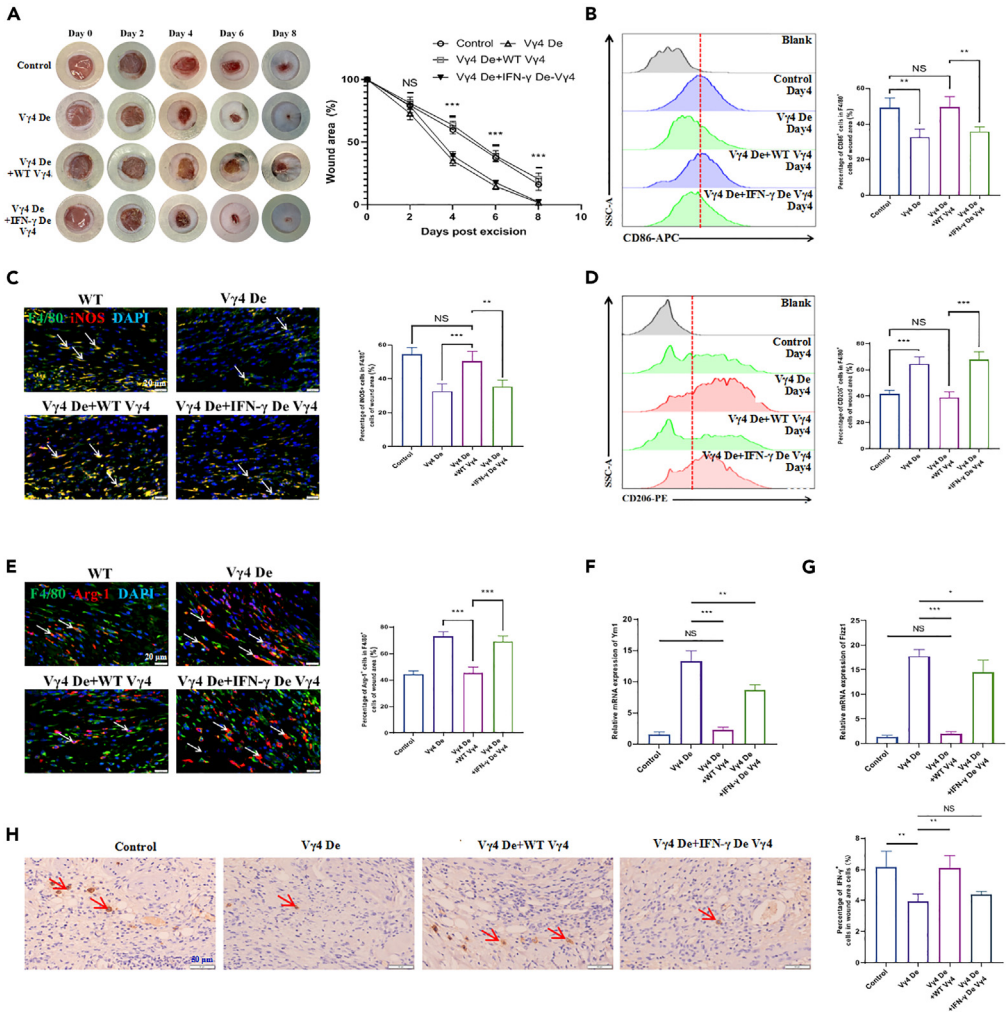

Figure 5. Vγ4 T cells secreting IFN-γ play critical role in impeding the M2 polarization and wound healing

(A) Macroscopic quantification of wound closure kinetics in Control mice, Vγ4 De mice, Vγ4 De+WT Vγ4 mice, and Vγ4 De+IFN-γ De Vγ4 mice (n = 10, 2 wounds/mouse, 5 mice/group).

(B) Flow cytometry quantifying $CD86^+$ frequency among wound macrophages on the 4^{th} day post-injury in the indicated four groups of mice, n = 4 mice per group compiled from two independent experiments.

(C) Immunofluorescence staining and quantification of $iNOS^+$ M1 macrophages in wound sections on the 4^{th} day post-injury in the indicated four groups of mice (n = 4 mice per group), scale bar, 20 μm.

(D) Flow cytometry quantifying $CD206^+$ frequency among wound macrophages on the 4^{th} day post-injury in the indicated four groups of mice, n = 4 mice per group compiled from two independent experiments.

(E) Immunofluorescence staining and quantification of $Arg1^+$ M2 macrophages in wound sections on 4^{th} day post-injury in the indicated four groups of mice (n = 4 mice per group), scale bar, 20 μm.

(F) qPCR analysis of Ym1 mRNA expression in wound lysates on the 4^{th} day post-injury in the indicated four groups of mice, n = 4 mice per group compiled from two independent experiments.

(G) Quantitative PCR (qPCR) analysis of Fizz1 mRNA expression in wound lysates on the 4^{th} day post-injury in the indicated four groups of mice, n = 4 mice per group compiled from two independent experiments.

(H) Immunohistochemical staining and quantification of IFN-γ^+ cells in wound sections on the 4^{th} day post-injury in the indicated four groups of mice, n = 4 mice per group compiled from two independent experiments, scale bar, 50 μm. Bars show the Mean ± SD. One-way ANOVA with Tukey's multiple comparisons test was applied to calculate the p value. *, $p < 0.05$; **, $p < 0.01$; ***, $p < 0.001$; NS, not significant. The arrows in the figures indicate the positive staining.

Translationally, strategies targeting $V\gamma4^+$ γδ T cells or downstream IFN-γ/monocyte pathways may hold promise to overcome pathological inflammation and enable healing in chronic wounds. The role of IFN-γ in wound healing remains controversial, IFN-γ KO (IFN-γ depleted) mice exhibited enhanced angiogenesis and accelerated wound healing,[83–85] while other research has discovered that defects of IFN-γ led to impaired wound closure in specific phases or IFN-γ-tethered materials promoted wound closure,[86,87] we speculated the different results were closely related to the local concentration and diverse stages of wound healing. Our findings bypassed the uncertainty of IFN-γ, and

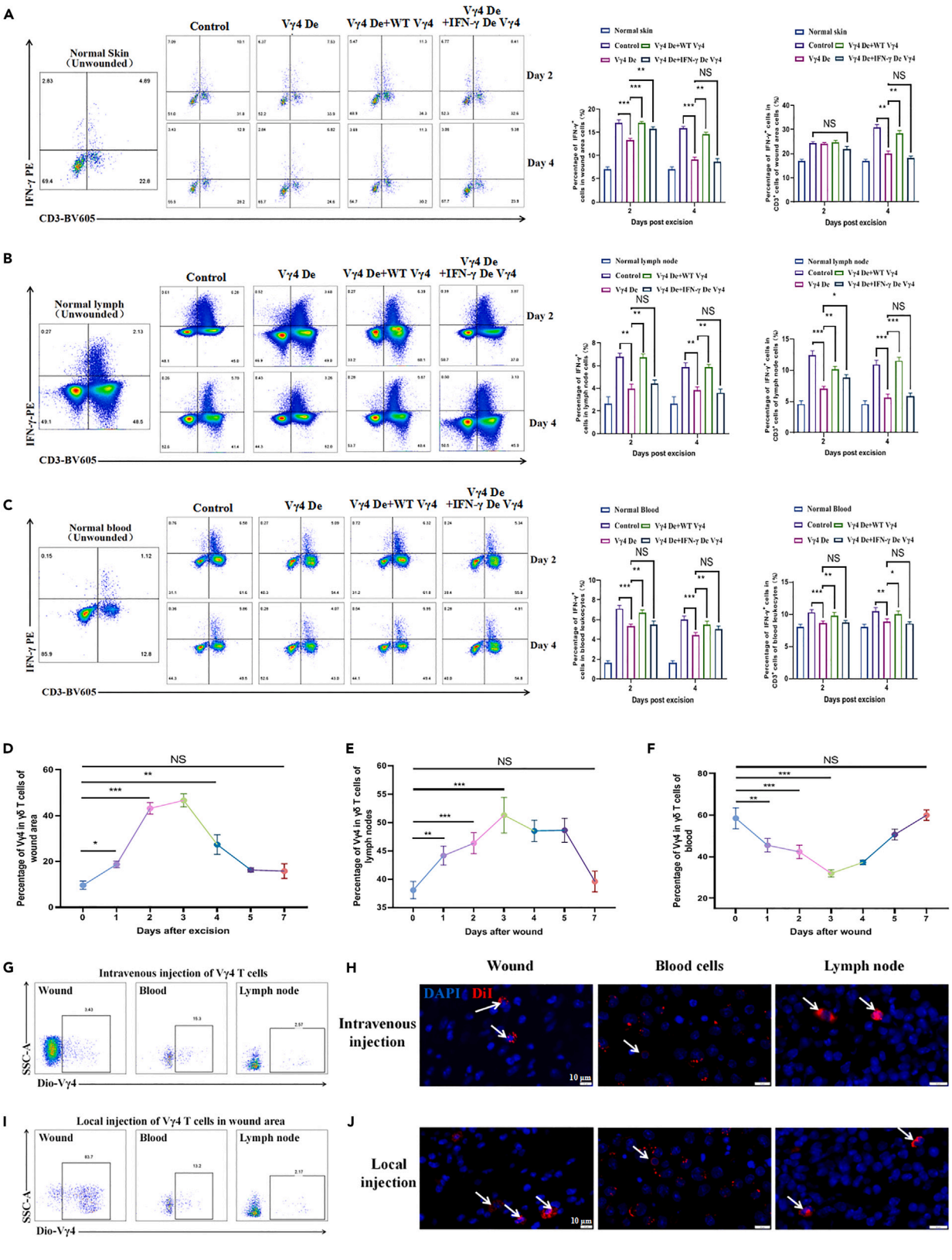
A
Control
Vγ4 De
Vγ4 De+WT Vγ4
Vγ4 De +IFN-γ De Vγ4
Normal Skin (Unwounded)
Day 2
Day 4
IFN-γ PE
CD3-BV605
Normal skin
Control
Vγ4 De+WT Vγ4
Vγ4 De
Vγ4 De+IFN-γ De Vγ4
Percentage of IFN-γ+ cells in wound area cells (%)
Percentage of IFN-γ+ cells in CD3+ cells of wound area cells (%)
Days post excision
B
Normal lymph (Unwounded)
Normal lymph node
Percentage of IFN-γ+ cells in lymph node cells (%)
Percentage of IFN-γ+ cells in CD3+ cells of lymph node cells (%)
C
Normal blood (Unwounded)
Normal Blood
Percentage of IFN-γ+ cells in blood leukocytes (%)
Percentage of IFN-γ+ cells in CD3+ cells of blood leukocytes (%)
D
Percentage of Vγ4 in γδ T cells of wound area
Days after excision
E
Percentage of Vγ4 in γδ T cells of lymph nodes
Days after wound
F
Percentage of Vγ4 in γδ T cells of blood
Days after wound
G
Intravenous injection of Vγ4 T cells
Wound
Blood
Lymph node
SSC-A
Dio-Vγ4
H
Wound
Blood cells
Lymph node
Intravenous injection
DAPI
DiI
10 μm
I
Local injection of Vγ4 T cells in wound area
J
Local injection

Figure 6. Vγ4 T cells in the wound, blood and lymph node form a cycle to license IFN-γ$^+$ cells

(A) Flow cytometry quantifying IFN-γ$^+$ cell frequency among all cells or CD3$^+$ cells in normal skin digest, and wound digests on the 2nd and 4th days post-injury of the indicated four groups (Control mice, Vγ4 De mice, Vγ4 De + WT Vγ4 mice, and Vγ4 De + IFN-γ De Vγ4 mice), n = 4 mice per group compiled from two independent experiments.

(B) Flow cytometry quantifying IFN-γ$^+$ cells frequency among all cells or CD3$^+$ cells in normal lymph node digest, and wound draining lymph node digests on the 2nd and 4th days post-injury of the indicated four groups, n = 4 mice per group compiled from two independent experiments.

(C) Flow cytometry quantifying IFN-γ$^+$ cell frequency among all cells or CD3$^+$ cells in normal blood, and blood on 2nd and 4th day post-injury of the indicated four groups, n = 4 mice per group compiled from two independent experiments.

(D–F) Flow cytometry quantifying frequency of Vγ4$^+$ cells among γδ TCR$^+$ cells in wound digests, lymph node digest and blood cells on indicated days post-injury (days 1,2,3,4,5, and 7), n = 5 mice per time point compiled from two independent experiments.

(G) Flow cytometry quantifying infiltration of fluorescently labeled Vγ4 T cells in wound digests, blood and lymph node digests on 3rd day post-injury after intravenous adoptive transfer on the 2nd day post-injury. n = 3 mice compiled from two independent experiments.

(H) Fluorescence microscopy visualizing of fluorescently labeled Vγ4 T cells (red) in wound, blood cells and lymph node on the 3rd post-injury after intravenous adoptive transfer on the 2nd day post-injury, nuclei counterstained with DAPI (blue), scale bar, 10 μm, n = 3 mice compiled from two independent experiments.

(I) Flow cytometry quantifying infiltration of fluorescently labeled Vγ4 T cells in wound digests, blood and lymph node digests on the 3rd post-injury after local adoptive transfer on the 2nd day post-injury. n = 3 mice compiled from two independent experiments.

(J) Fluorescence microscopy visualizing of fluorescently labeled Vγ4 T cells (red) in the wound bed, blood cells and lymph node on the 3rd post-injury after local adoptive transfer on the 2nd day post-injury, nuclei counterstained with DAPI (blue), scale bar, 10 μm, n = 3 mice compiled from two independent experiments. Bars show the Mean ± SD. One-way ANOVA with Tukey's multiple comparisons test was applied to calculate the p value (A, B, C, D, E, and F). *, $p < 0.05$; **, $p < 0.01$; ***, $p < 0.001$; NS, not significant. The arrows in Figures 6H and 6J indicate the positive staining of Vγ4 T cells (red).

provided a proof-of-concept validation that Vγ4$^+$ γδ T cell was the pivotal commander in amplifying IFN-γ and macrophage phenotypic switching, which could be a potential therapeutic target. Advancing these approaches from mice to human patients remains challenging but warrants further investigation. Possibilities include antibody-mediated γδ T cell depletion, concentration-dependent IFN-γ adjustment, and inhibition of Ly6C$^+$ monocyte generation or recruitment. More broadly, similar immunopathological mechanisms may be operative across diverse tissue healing and inflammatory disorders where γδ T cell subsets have been implicated, including pulmonary fibrosis,[88,89] inflammatory bowel disease,[90,91] liver fibrosis,[92,93] and autoimmunity disease.[94]

In conclusion, this study provides seminal mechanistic insights into the multi-tiered orchestration of macrophage activation trajectories during skin repair by motile Vγ4$^+$ γδ T cells through sophisticated IFN-γ conditioning. The findings illuminate an innate lymphocyte-myeloid cell signaling circuit regulating the immunological setpoints that calibrate cutaneous inflammation. Moving forward, deeper interrogation of the factors governing Vγ4$^+$ γδ T cell mobilization, activation, trafficking patterns, and downstream functional interactions will continue advancing the understanding of their versatile tissue-reparative and pathological properties. On the translational front, therapeutically harnessing Vγ4$^+$ γδ T cell or IFN-γ signaling plasticity represents a promising approach to enhance macrophage immunometabolism and resolve inflammation in difficult-to-heal wounds.

Limitations of the study

Firstly, the dynamics of Vγ4$^+$ γδ T cell responses defined here were primarily in acute wound settings over a 1–2 weeks time frame. It will be essential to extend the analysis temporally into later healing phases encompassing remodeling or other chronic wound scenarios. Secondly, precisely defining the activation cues triggering Vγ4$^+$ γδ T cell mobilization and IFN-γ induction after injury requires further elucidation. Candidates include damage-associated molecular patterns like ATP (Adenosine triphosphate) and IL-1 (Interleukin-1) family cytokines. Thirdly, dissecting the mechanisms of Vγ4$^+$ γδ T cell interactions with lymphocytes, and myeloid precursors could unveil additional druggable immunomodulatory pathways. Additionally, exploring whether strategies targeting Vγ4$^+$ γδ T cell trafficking, viability, or effector functions can overcome macrophage-driven inflammation during pathogenic wound healing will provide further preclinical validation. In addition, scRNA-seq (single-cell RNA sequencing) was not conducted in this paper, as we all know, scRNA-seq is an efficient approach allowing for unbiased single-cell transcriptome profiling[95] to characterize distinct cell subsets,[96] identify the heterogeneity of a population[97] and dissect cell fate branch points.[98] In our further study, the scRNA-seq will be conducted to find and lock onto the target regulated subsets of macrophages. Lastly, in consideration of the large fluctuations in gonadal hormones over the 4-day estrous cycle (equivalent of the human menstrual cycle) of female mice, only male mice were used in this paper as in most of other studies.[99] Actually, the prevailing argument that the inclusion of females introduces greater variability or increased dispersion in experiments is outdated. Studies in recent years have suggested data obtained from female rodents are not more variable than that obtained from males in many aspects, even in the absence of controlling for hormonal levels in females;[99] moreover, responses to many disorders or diseases differed more or less between males and females.[100] So, in our future studies, we will discard this conventional prejudice, and include females and males equally in our experiments to make our experiments more reasonable.

STAR★METHODS

Detailed methods are provided in the online version of this paper and include the following:

- KEY RESOURCES TABLE
- RESOURCE AVAILABILITY

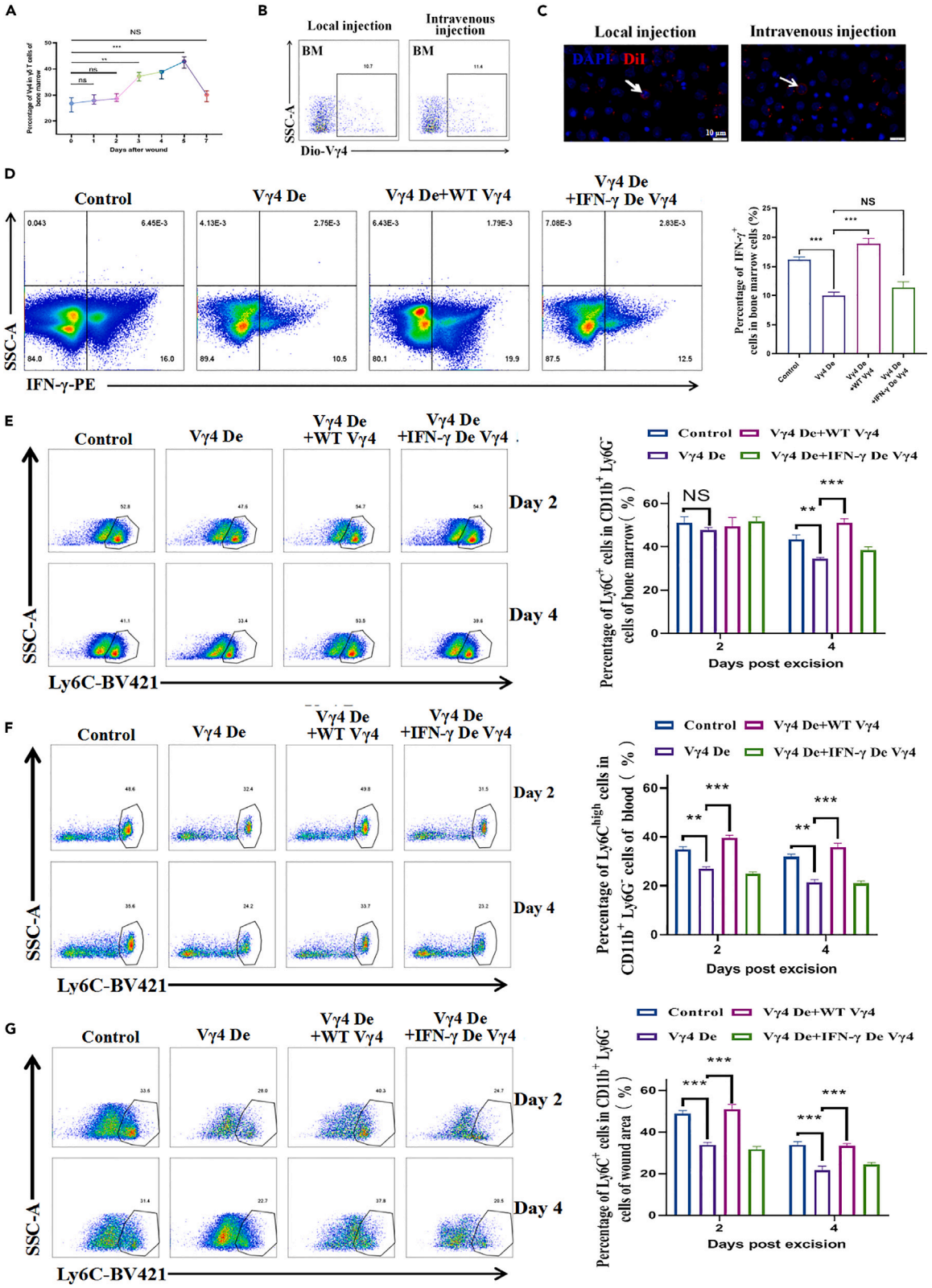
A
NS
***
**
ns
ns
Percentage of Vγ4 in γδ T cells of bone marrow
Days after wound
B
Local injection
Intravenous injection
BM
BM
SSC-A
Dio-Vγ4
C
Local injection
Intravenous injection
DAPI
DiI
10 μm
D
Control
Vγ4 De
Vγ4 De+WT Vγ4
Vγ4 De +IFN-γ De Vγ4
0.043
6.45E-3
84.0
16.0
4.13E-3
2.75E-3
89.4
10.5
6.43E-3
1.79E-3
80.1
19.9
7.08E-3
2.83E-3
87.5
12.5
SSC-A
IFN-γ-PE
NS
***
***
Percentage of IFN-γ+ cells in bone marrow cells (%)
Control
Vγ4 De
Vγ4 De +WT Vγ4
Vγ4 De +IFN-γ De Vγ4
E
Control
Vγ4 De
Vγ4 De +WT Vγ4
Vγ4 De +IFN-γ De Vγ4
Day 2
Day 4
SSC-A
Ly6C-BV421
Control
Vγ4 De+WT Vγ4
Vγ4 De
Vγ4 De+IFN-γ De Vγ4
NS
**
***
***
Percentage of Ly6C+ cells in CD11b+ Ly6G- cells of bone marrow (%)
Days post excision
F
Control
Vγ4 De
Vγ4 De +WT Vγ4
Vγ4 De +IFN-γ De Vγ4
Day 2
Day 4
SSC-A
Ly6C-BV421
Control
Vγ4 De+WT Vγ4
Vγ4 De
Vγ4 De+IFN-γ De Vγ4
**
***
**
***
Percentage of Ly6Chigh cells in CD11b+ Ly6G- cells of blood (%)
Days post excision
G
Control
Vγ4 De
Vγ4 De +WT Vγ4
Vγ4 De +IFN-γ De Vγ4
Day 2
Day 4
SSC-A
Ly6C-BV421
Control
Vγ4 De+WT Vγ4
Vγ4 De
Vγ4 De+IFN-γ De Vγ4
***
***
***
***
Percentage of Ly6C+ cells in CD11b+ Ly6G- cells of wound area (%)
Days post excision

Figure 7. Vγ4 T cells infiltrate into the bone marrow and influence monocytes

(A) Flow cytometry quantifying frequency of Vγ4$^+$ cells among γδ TCR$^+$ cells in bone marrow on indicated days post-injury (days 1,2,3,4,5, and 7). n = 5 mice per time point compiled from two independent experiments.

(B) Flow cytometry quantifying infiltration of fluorescently labeled Vγ4 T cells in bone marrow cells on the 3rd post-injury after local or intravenous adoptive transfer on the 2nd day post-injury, n = 3 mice compiled from two independent experiments.

(C) Fluorescence microscopy visualizing of fluorescently labeled Vγ4 T cells (red) in bone marrow cells on the 3rd post-injury after local or intravenous adoptive transfer on the 2nd day post-injury, nuclei counterstained with DAPI (blue), n = 3 mice compiled from two independent experiments, scale bar, 10 μm.

(D) Flow cytometry quantifying frequency of IFN-γ$^+$ cells among all cells in bone marrow on the 4th day post-injury of the indicated four groups (Control mice, Vγ4 De mice, Vγ4 De + WT Vγ4 mice, and Vγ4 De + IFN-γ De Vγ4 mice). n = 3 mice per group.

(E) Flow cytometry quantifying frequencies of Ly6C$^+$ monocytes among CD11b$^+$Ly6G$^-$ cells of bone marrow on the 2nd and 4th days post-injury of the indicated four groups. n = 4 mice per group compiled from two independent experiments.

(F) Flow cytometry quantifying frequencies of Ly6C^{high} monocytes among CD11b$^+$Ly6G$^-$ cells of blood on the 2nd and 4th days post-injury of the indicated four groups. n = 4 mice per group compiled from two independent experiments.

(G) Flow cytometry quantifying frequencies of Ly6C$^+$ monocytes among CD11b$^+$Ly6G$^-$ cells of wound area on the 2nd and 4th days post-injury of the indicated four groups. n = 4 mice per group compiled from two independent experiments. Bars show the Mean ± SD. One-way ANOVA with Tukey's multiple comparisons test was applied to calculate the p value (A, D, E, F, and G). *, $p < 0.05$; **, $p < 0.01$; ***, $p < 0.001$; NS, not significant. The arrows in the Figure 7C indicate the positive staining of Vγ4 T cells (red).

SUPPLEMENTAL INFORMATION

Supplemental information can be found online at https://doi.org/10.1016/j.isci.2024.109545.

ACKNOWLEDGMENTS

We thank all members of W. He and G.L. laboratories for support in the experiments. This work was supported by funds from the National Natural Science Foundation of China of China (No. 82172232 to W. He., No. 81920108022, 2021YFA1101100 to G.L., NO. 32370921 to J.H., NO. 82202464 to Y.C.).

AUTHOR CONTRIBUTIONS

W. Hu drafted the manuscript and participated in the study design and supervision, X.Z. conducted the western blot and qPCR. Zhongyang Liu and J.Y. collected the data and completed the statistics. H.S. conducted the flow cytometry. Zhihui Liu, C.C., and R.S. took part in the *in vitro* experiments. Y.C., Y.L., and X.H. cultured the cells *in vitro*. Y.H. and W.Y. participated in the *in vivo* experiments; X.C. conducted the immunofluorescence microscopy, D.F. and L.Y. generated the full-thickness excisional wounds; J.H. made some valuable suggestions about manuscript structure, W. He and G.L. evaluated and reviewed manuscript structure, ideas and science. All authors have read and approved the final manuscript.

DECLARATION OF INTERESTS

The authors declare no competing interest.

Received: October 25, 2023
Revised: February 8, 2024
Accepted: March 18, 2024
Published: March 21, 2024

REFERENCES

1. Rodrigues, M., Kosaric, N., Bonham, C.A., and Gurtner, G.C. (2019). Wound Healing: A Cellular Perspective. Physiol. Rev. *99*, 665–706. https://doi.org/10.1152/physrev.00067.2017.
2. Koh, T.J., and DiPietro, L.A. (2011). Inflammation and wound healing: the role of the macrophage. Expet Rev. Mol. Med. *13*, e23. https://doi.org/10.1017/S1462399411001943.
3. Martin, P., and Nunan, R. (2015). Cellular and molecular mechanisms of repair in acute and chronic wound healing. Br. J. Dermatol. *173*, 370–378. https://doi.org/10.1111/bjd.13954.
4. Eming, S.A., Krieg, T., and Davidson, J.M. (2007). Inflammation in wound repair: molecular and cellular mechanisms. J. Invest. Dermatol. *127*, 514–525. https://doi.org/10.1038/sj.jid.5700701.
5. Tacke, F., and Zimmermann, H.W. (2014). Macrophage heterogeneity in liver injury and fibrosis. J. Hepatol. *60*, 1090–1096. https://doi.org/10.1016/j.jhep.2013.12.025.
6. Sharifiaghdam, M., Shaabani, E., Faridi-Majidi, R., De Smedt, S.C., Braeckmans, K., and Fraire, J.C. (2022). Macrophages as a therapeutic target to promote diabetic wound healing. Mol. Ther. *30*, 2891–2908. https://doi.org/10.1016/j.ymthe.2022.07.016.
7. Hassanshahi, A., Moradzad, M., Ghalamkari, S., Fadaei, M., Cowin, A.J., and Hassanshahi, M. (2022). Macrophage-Mediated Inflammation in Skin Wound Healing. Cells *11*, 2953. https://doi.org/10.3390/cells11192953.
8. Krzyszczyk, P., Schloss, R., Palmer, A., and Berthiaume, F. (2018). The Role of Macrophages in Acute and Chronic Wound Healing and Interventions to Promote Pro-wound Healing Phenotypes. Front. Physiol. *9*, 419. https://doi.org/10.3389/fphys.2018.00419.
9. Li, M., Hou, Q., Zhong, L., Zhao, Y., and Fu, X. (2021). Macrophage Related Chronic Inflammation in Non-Healing Wounds. Front. Immunol. *12*, 681710. https://doi.org/10.3389/fimmu.2021.681710.
10. Novak, M.L., and Koh, T.J. (2013). Macrophage phenotypes during tissue repair. J. Leukoc. Biol. *93*, 875–881. https://doi.org/10.1189/jlb.1012512.
11. Xu, X., Gu, S., Huang, X., Ren, J., Gu, Y., Wei, C., Lian, X., Li, H., Gao, Y., Jin, R., et al. (2020). The role of macrophages in the formation of hypertrophic scars and keloids. Burns Trauma *8*, tkaa006. https://doi.org/10.1093/burnst/tkaa006.
12. Slauch, J.M. (2011). How does the oxidative burst of macrophages kill bacteria? Still an open question. Mol. Microbiol. *80*, 580–583. https://doi.org/10.1111/j.1365-2958.2011.07612.x.
13. Lucas, T., Waisman, A., Ranjan, R., Roes, J., Krieg, T., Müller, W., Roers, A., and Eming, S.A. (2010). Differential roles of macrophages in diverse phases of skin repair. J. Immunol. *184*, 3964–3977. https://doi.org/10.4049/jimmunol.0903356.
14. Galli, S.J., Borregaard, N., and Wynn, T.A. (2011). Phenotypic and functional plasticity of cells of innate immunity: macrophages, mast cells and neutrophils. Nat. Immunol. *12*, 1035–1044. https://doi.org/10.1038/ni.2109.
15. Ganesh, G.V., and Ramkumar, K.M. (2020). Macrophage mediation in normal and diabetic wound healing responses. Inflamm. Res. *69*, 347–363. https://doi.org/10.1007/s00011-020-01328-y.
16. Wu, X., He, W., Mu, X., Liu, Y., Deng, J., Liu, Y., and Nie, X. (2022). Macrophage polarization in diabetic wound healing. Burns Trauma *10*, tkac051. https://doi.org/10.1093/burnst/tkac051.
17. Munoz, L.D., Sweeney, M.J., and Jameson, J.M. (2020). Skin Resident gammadelta T Cell Function and Regulation in Wound Repair. Int. J. Mol. Sci. *21*, 9286. https://doi.org/10.3390/ijms21239286.
18. Toulon, A., Breton, L., Taylor, K.R., Tenenhaus, M., Bhavsar, D., Lanigan, C., Rudolph, R., Jameson, J., and Havran, W.L. (2009). A role for human skin-resident T cells in wound healing. J. Exp. Med. *206*, 743–750. https://doi.org/10.1084/jem.20081787.
19. Short, W.D., Wang, X., and Keswani, S.G. (2022). The Role of T Lymphocytes in Cutaneous Scarring. Adv. Wound Care *11*, 121–131. https://doi.org/10.1089/wound.2021.0059.
20. Chien, Y.H., Meyer, C., and Bonneville, M. (2014). gammadelta T cells: first line of defense and beyond. Annu. Rev. Immunol. *32*, 121–155. https://doi.org/10.1146/annurev-immunol-032713-120216.
21. Constantinides, M.G., and Belkaid, Y. (2021). Early-life imprinting of unconventional T cells and tissue homeostasis. Science *374*, eabf0095. https://doi.org/10.1126/science.abf0095.
22. Chen, C., Meng, Z., Ren, H., Zhao, N., Shang, R., He, W., and Hao, J. (2021). The molecular mechanisms supporting the homeostasis and activation of dendritic epidermal T cell and its role in promoting wound healing. Burns Trauma *9*, tkab009. https://doi.org/10.1093/burnst/tkab009.
23. Mensurado, S., Blanco-Domínguez, R., and Silva-Santos, B. (2023). The emerging roles of gammadelta T cells in cancer immunotherapy. Nat. Rev. Clin. Oncol. *20*, 178–191. https://doi.org/10.1038/s41571-022-00722-1.
24. Wang, Y., Bai, Y., Li, Y., Liang, G., Jiang, Y., Liu, Z., Liu, M., Hao, J., Zhang, X., Hu, X., et al. (2017). IL-15 Enhances Activation and IGF-1 Production of Dendritic Epidermal T Cells to Promote Wound Healing in Diabetic Mice. Front. Immunol. *8*, 1557. https://doi.org/10.3389/fimmu.2017.01557.
25. Li, Y., Wang, Y., Zhou, L., Liu, M., Liang, G., Yan, R., Jiang, Y., Hao, J., Zhang, X., Hu, X., et al. (2018). Vgamma4 T Cells Inhibit the Pro-healing Functions of Dendritic Epidermal T Cells to Delay Skin Wound Closure Through IL-17A. Front. Immunol. *9*, 240. https://doi.org/10.3389/fimmu.2018.00240.
26. Sun, G., Yang, S., Cao, G., Wang, Q., Hao, J., Wen, Q., Li, Z., So, K.F., Liu, Z., Zhou, S., et al. (2018). gammadelta T cells provide the early source of IFN-gamma to aggravate lesions in spinal cord injury. J. Exp. Med. *215*, 521–535. https://doi.org/10.1084/jem.20170686.
27. Ribot, J.C., Lopes, N., and Silva-Santos, B. (2021). gammadelta T cells in tissue physiology and surveillance. Nat. Rev. Immunol. *21*, 221–232. https://doi.org/10.1038/s41577-020-00452-4.
28. Ren, H., Li, W., Liu, X., and Zhao, N. (2022). gammadelta T cells: The potential role in liver disease and implications for cancer immunotherapy. J. Leukoc. Biol. *112*, 1663–1668. https://doi.org/10.1002/JLB.5MR0822-733RRR.
29. Li, Y., Wu, J., Luo, G., and He, W. (2018). Functions of Vgamma4 T Cells and Dendritic Epidermal T Cells on Skin Wound Healing. Front. Immunol. *9*, 1099. https://doi.org/10.3389/fimmu.2018.01099.
30. Song, Y., Hu, W., Xiao, Y., Li, Y., Wang, X., He, W., Hou, J., Liu, Y., Liang, G., and Huang, C. (2020). Keratinocyte growth factor ameliorates mycophenolate mofetil-induced intestinal barrier disruption in mice. Mol. Immunol. *124*, 61–69. https://doi.org/10.1016/j.molimm.2020.04.012.
31. Cai, Y., Xue, F., Quan, C., Qu, M., Liu, N., Zhang, Y., Fleming, C., Hu, X., Zhang, H.G., Weichselbaum, R., et al. (2019). A Critical Role of the IL-1beta-IL-1R Signaling Pathway in Skin Inflammation and Psoriasis Pathogenesis. J. Invest. Dermatol. *139*, 146–156. https://doi.org/10.1016/j.jid.2018.07.025.
32. Cruz, M.S., Diamond, A., Russell, A., and Jameson, J.M. (2018). Human alphabeta and gammadelta T Cells in Skin Immunity and Disease. Front. Immunol. *9*, 1304. https://doi.org/10.3389/fimmu.2018.01304.
33. Havran, W.L., Chien, Y.H., and Allison, J.P. (1991). Recognition of self antigens by skin-derived T cells with invariant gamma delta antigen receptors. Science *252*, 1430–1432. https://doi.org/10.1126/science.1828619.
34. Hu, W., Zhang, X., Sheng, H., Liu, Z., Chen, Y., Huang, Y., He, W., and Luo, G. (2023). The mutual regulation between gammadelta T cells and macrophages during wound

healing. J. Leukoc. Biol. qiad087. https://doi.org/10.1093/jleuko/qiad087.
35. Daley, D., Zambirinis, C.P., Seifert, L., Akkad, N., Mohan, N., Werba, G., Barilla, R., Torres-Hernandez, A., Hundeyin, M., Mani, V.R.K., et al. (2016). gammadelta T Cells Support Pancreatic Oncogenesis by Restraining alphabeta T Cell Activation. Cell *166*, 1485–1499.e15. https://doi.org/10.1016/j.cell.2016.07.046.
36. Castro, C.D., Boughter, C.T., Broughton, A.E., Ramesh, A., and Adams, E.J. (2020). Diversity in recognition and function of human gammadelta T cells. Immunol. Rev. *298*, 134–152. https://doi.org/10.1111/imr.12930.
37. Song, Y., Li, Y., Xiao, Y., Hu, W., Wang, X., Wang, P., Zhang, X., Yang, J., Huang, Y., He, W., and Huang, C. (2019). Neutralization of interleukin-17A alleviates burn-induced intestinal barrier disruption via reducing pro-inflammatory cytokines in a mouse model. Burns Trauma *7*, 37. https://doi.org/10.1186/s41038-019-0177-9.
38. Havran, W.L., and Jameson, J.M. (2010). Epidermal T cells and wound healing. J. Immunol. *184*, 5423–5428. https://doi.org/10.4049/jimmunol.0902733.
39. Xu, P., Fu, X., Xiao, N., Guo, Y., Pei, Q., Peng, Y., Zhang, Y., and Yao, M. (2017). Involvements of gammadeltaT Lymphocytes in Acute and Chronic Skin Wound Repair. Inflammation *40*, 1416–1427. https://doi.org/10.1007/s10753-017-0585-6.
40. Hou, Y., Wei, D., Zhang, Z., Lei, T., Li, S., Bao, J., Guo, H., Tan, L., Xie, X., Zhuang, Y., et al. (2024). Downregulation of nutrition sensor GCN2 in macrophages contributes to poor wound healing in diabetes. Cell Rep. *43*, 113658. https://doi.org/10.1016/j.celrep.2023.113658.
41. Karnam, K., Sedmaki, K., Sharma, P., Mahale, A., Ghosh, B., and Kulkarni, O.P. (2023). Pharmacological blockade of HDAC3 accelerates diabetic wound healing by regulating macrophage activation. Life Sci. *321*, 121574. https://doi.org/10.1016/j.lfs.2023.121574.
42. Chen, C., Tang, Y., Zhu, X., Yang, J., Liu, Z., Chen, Y., Wang, J., Shang, R., Zheng, W., Zhang, X., et al. (2023). P311 Promotes IL-4 Receptor–Mediated M2 Polarization of Macrophages to Enhance Angiogenesis for Efficient Skin Wound Healing. J. Invest. Dermatol. *143*, 648–660.e6. https://doi.org/10.1016/j.jid.2022.09.659.
43. Koo, J.H., Jang, H.Y., Lee, Y., Moon, Y.J., Bae, E.J., Yun, S.K., and Park, B.H. (2019). Myeloid cell-specific sirtuin 6 deficiency delays wound healing in mice by modulating inflammation and macrophage phenotypes. Exp. Mol. Med. *51*, 1–10. https://doi.org/10.1038/s12276-019-0248-9.
44. Zhang, Y., and Lu, Q. (2023). Immune cells in skin inflammation, wound healing and skin cancer. J. Leukoc. Biol. qiad107. https://doi.org/10.1093/jleuko/qiad107.
45. Jakovija, A., and Chtanova, T. (2023). Skin immunity in wound healing and cancer. Front. Immunol. *14*, 1060258. https://doi.org/10.3389/fimmu.2023.1060258.
46. Vivier, E., Artis, D., Colonna, M., Diefenbach, A., Di Santo, J.P., Eberl, G., Koyasu, S., Locksley, R.M., McKenzie, A.N.J., Mebius, R.E., et al. (2018). Innate Lymphoid Cells: 10 Years On. Cell *174*, 1054–1066. https://doi.org/10.1016/j.cell.2018.07.017.
47. Klose, C.S.N., and Artis, D. (2016). Innate lymphoid cells as regulators of immunity, inflammation and tissue homeostasis. Nat. Immunol. *17*, 765–774. https://doi.org/10.1038/ni.3489.
48. Rak, G.D., Osborne, L.C., Siracusa, M.C., Kim, B.S., Wang, K., Bayat, A., Artis, D., and Volk, S.W. (2016). IL-33-Dependent Group 2 Innate Lymphoid Cells Promote Cutaneous Wound Healing. J. Invest. Dermatol. *136*, 487–496. https://doi.org/10.1038/JID.2015.406.
49. Li, Y., Lin, S., Xiong, S., and Xie, Q. (2022). Recombinant Expression of Human IL-33 Protein and Its Effect on Skin Wound Healing in Diabetic Mice. Bioengineering (Basel) *9*, 734. https://doi.org/10.3390/bioengineering9120734.
50. Ferrante, C.J., and Leibovich, S.J. (2012). Regulation of Macrophage Polarization and Wound Healing. Adv. Wound Care *1*, 10–16. https://doi.org/10.1089/wound.2011.0307.
51. Chen, C., Liu, T., Tang, Y., Luo, G., Liang, G., and He, W. (2023). Epigenetic regulation of macrophage polarization in wound healing. Burns Trauma *11*, tkac057. https://doi.org/10.1093/burnst/tkac057.
52. Abou-El-Hassan, H., Rezende, R.M., Izzy, S., Gabriely, G., Yahya, T., Tatematsu, B.K., Habashy, K.J., Lopes, J.R., de Oliveira, G.L.V., Maghzi, A.H., et al. (2023). Vgamma1 and Vgamma4 gamma-delta T cells play opposing roles in the immunopathology of traumatic brain injury in males. Nat. Commun. *14*, 4286. https://doi.org/10.1038/s41467-023-39857-9.
53. Wan, J., Zhang, Q., Hao, Y., Tao, Z., Song, W., Chen, S., Qin, L., Song, W., and Shan, Y. (2023). Infiltrated IL-17A-producing gamma delta T cells play a protective role in sepsis-induced liver injury and are regulated by CCR6 and gut commensal microbes. Front. Cell. Infect. Microbiol. *13*, 1149506. https://doi.org/10.3389/fcimb.2023.1149506.
54. Hammerich, L., Bangen, J.M., Govaere, O., Zimmermann, H.W., Gassler, N., Huss, S., Liedtke, C., Prinz, I., Lira, S.A., Luedde, T., et al. (2014). Chemokine receptor CCR6-dependent accumulation of gammadelta T cells in injured liver restricts hepatic inflammation and fibrosis. Hepatology *59*, 630–642. https://doi.org/10.1002/hep.26697.
55. Fischer, M.A., Golovchenko, N.B., and Edelblum, K.L. (2020). gammadelta T cell migration: Separating trafficking from surveillance behaviors at barrier surfaces. Immunol. Rev. *298*, 165–180. https://doi.org/10.1111/imr.12915.
56. Dovi, J.V., He, L.K., and DiPietro, L.A. (2003). Accelerated wound closure in neutrophil-depleted mice. J. Leukoc. Biol. *73*, 448–455. https://doi.org/10.1189/jlb.0802406.
57. Oppeltz, R.F., Rani, M., Zhang, Q., and Schwacha, M.G. (2012). Gamma delta (gammadelta) T-cells are critical in the up-regulation of inducible nitric oxide synthase at the burn wound site. Cytokine *60*, 528–534. https://doi.org/10.1016/j.cyto.2012.07.003.
58. Schwacha, M.G. (2003). Macrophages and post-burn immune dysfunction. Burns *29*, 1–14. https://doi.org/10.1016/s0305-4179(02)00187-0.
59. Li, S., Yang, P., Ding, X., Zhang, H., Ding, Y., and Tan, Q. (2022). Puerarin improves diabetic wound healing via regulation of macrophage M2 polarization phenotype. Burns Trauma *10*, tkac046. https://doi.org/10.1093/burnst/tkac046.
60. Locati, M., Curtale, G., and Mantovani, A. (2020). Diversity, Mechanisms, and Significance of Macrophage Plasticity. Annu. Rev. Pathol. *15*, 123–147. https://doi.org/10.1146/annurev-pathmechdis-012418-012718.
61. Aitcheson, S.M., Frentiu, F.D., Hurn, S.E., Edwards, K., and Murray, R.Z. (2021). Skin Wound Healing: Normal Macrophage Function and Macrophage Dysfunction in Diabetic Wounds. Molecules *26*, 4917. https://doi.org/10.3390/molecules26164917.
62. Nakanishi, Y., Sato, T., Takahashi, K., and Ohteki, T. (2018). IFN-gamma-dependent epigenetic regulation instructs colitogenic monocyte/macrophage lineage differentiation *in vivo*. Mucosal Immunol. *11*, 871–880. https://doi.org/10.1038/mi.2017.104.
63. Kusaka, Y., Kajiwara, C., Shimada, S., Ishii, Y., Miyazaki, Y., Inase, N., Standiford, T.J., and Tateda, K. (2018). Potential Role of Gr-1+ CD8+ T Lymphocytes as a Source of Interferon-gamma and M1/M2 Polarization during the Acute Phase of Murine Legionella pneumophila Pneumonia. J. Innate Immun. *10*, 328–338. https://doi.org/10.1159/000490585.
64. Schmit, T., Guo, K., Tripathi, J.K., Wang, Z., McGregor, B., Klomp, M., Ambigapathy, G., Mathur, R., Hur, J., Pichichero, M., et al. (2022). Interferon-gamma promotes monocyte-mediated lung injury during influenza infection. Cell Rep. *38*, 110456. https://doi.org/10.1016/j.celrep.2022.110456.
65. Li, Y.H., Zhang, Y., Pan, G., Xiang, L.X., Luo, D.C., and Shao, J.Z. (2022). Occurrences and Functions of Ly6C(hi) and Ly6C(lo) Macrophages in Health and Disease. Front. Immunol. *13*, 901672. https://doi.org/10.3389/fimmu.2022.901672.
66. Hoeffel, G., Debroas, G., Roger, A., Rossignol, R., Gouilly, J., Laprie, C., Chasson, L., Barbon, P.V., Balsamo, A., Reynders, A., et al. (2021). Sensory neuron-derived TAFA4 promotes macrophage tissue repair functions. Nature *594*, 94–99. https://doi.org/10.1038/s41586-021-03563-7.
67. Kimball, A., Schaller, M., Joshi, A., Davis, F.M., denDekker, A., Boniakowski, A., Bermick, J., Obi, A., Moore, B., Henke, P.K., et al. (2018). Ly6C(Hi) Blood Monocyte/Macrophage Drive Chronic Inflammation and Impair Wound Healing in Diabetes Mellitus. Arterioscler. Thromb. Vasc. Biol. *38*, 1102–1114. https://doi.org/10.1161/ATVBAHA.118.310703.
68. Pang, J., Urao, N., and Koh, T.J. (2020). Proliferation of Ly6C+ monocytes/macrophages contributes to their accumulation in mouse skin wounds. J. Leukoc. Biol. *107*, 551–560. https://doi.org/10.1002/JLB.3HI1119-389RRRR.
69. Elenkov, I.J., Wilder, R.L., Chrousos, G.P., and Vizi, E.S. (2000). The sympathetic nerve–an integrative interface between two supersystems: the brain and the immune system. Pharmacol. Rev. *52*, 595–638.
70. Ivanov, E., Akhmetshina, M., Erdiakov, A., and Gavrilova, S. (2023). Sympathetic System in Wound Healing: Multistage Control in Normal and Diabetic Skin. Int. J. Mol. Sci. *24*, 2045. https://doi.org/10.3390/ijms24032045.
71. O'Sullivan, S.T., Lederer, J.A., Horgan, A.F., Chin, D.H., Mannick, J.A., and Rodrick, M.L.

(1995). Major injury leads to predominance of the T helper-2 lymphocyte phenotype and diminished interleukin-12 production associated with decreased resistance to infection. Ann. Surg. *222*, 482–490. https://doi.org/10.1097/00000658-199522240-00006.

72. Udit, S., Blake, K., and Chiu, I.M. (2022). Somatosensory and autonomic neuronal regulation of the immune response. Nat. Rev. Neurosci. *23*, 157–171. https://doi.org/10.1038/s41583-021-00555-4.
73. Halin, C., Mora, J.R., Sumen, C., and von Andrian, U.H. (2005). In vivo imaging of lymphocyte trafficking. Annu. Rev. Cell Dev. Biol. *21*, 581–603. https://doi.org/10.1146/annurev.cellbio.21.122303.133159.
74. Greaves, N.S., Ashcroft, K.J., Baguneid, M., and Bayat, A. (2013). Current understanding of molecular and cellular mechanisms in fibroplasia and angiogenesis during acute wound healing. J. Dermatol. Sci. *72*, 206–217. https://doi.org/10.1016/j.jdermsci.2013.07.008.
75. Gurtner, G.C., Werner, S., Barrandon, Y., and Longaker, M.T. (2008). Wound repair and regeneration. Nature *453*, 314–321. https://doi.org/10.1038/nature07039.
76. Hu, W., Shang, R., Yang, J., Chen, C., Liu, Z., Liang, G., He, W., and Luo, G. (2022). Skin gammadelta T Cells and Their Function in Wound Healing. Front. Immunol. *13*, 875076. https://doi.org/10.3389/fimmu.2022.875076.
77. Taylor, K.R., Costanzo, A.E., and Jameson, J.M. (2011). Dysfunctional gammadelta T cells contribute to impaired keratinocyte homeostasis in mouse models of obesity. J. Invest. Dermatol. *131*, 2409–2418. https://doi.org/10.1038/jid.2011.241.
78. Liu, Z., Xu, Y., Zhang, X., Liang, G., Chen, L., Xie, J., Tang, J., Zhao, J., Shu, B., Qi, S., et al. (2016). Defects in dermal Vgamma4 gamma delta T cells result in delayed wound healing in diabetic mice. Am. J. Transl. Res. *8*, 2667–2680.
79. Latha, T.S., Reddy, M.C., Durbaka, P.V.R., Rachamallu, A., Pallu, R., and Lomada, D. (2014). gammadelta T Cell-Mediated Immune Responses in Disease and Therapy. Front. Immunol. *5*, 571. https://doi.org/10.3389/fimmu.2014.00571.
80. Kim, A., Lang, T., Xue, M., Wijewardana, A., Jackson, C., and Vandervord, J. (2017). The Role of Th-17 Cells and gammadelta T-Cells in Modulating the Systemic Inflammatory Response to Severe Burn Injury. Int. J. Mol. Sci. *18*, 758. https://doi.org/10.3390/ijms18040758.
81. Stark, M.A., Huo, Y., Burcin, T.L., Morris, M.A., Olson, T.S., and Ley, K. (2005). Phagocytosis of apoptotic neutrophils regulates granulopoiesis via IL-23 and IL-17. Immunity *22*, 285–294. https://doi.org/10.1016/j.immuni.2005.01.011.
82. Sindrilaru, A., Peters, T., Wieschalka, S., Baican, C., Baican, A., Peter, H., Hainzl, A., Schatz, S., Qi, Y., Schlecht, A., et al. (2011). An unrestrained proinflammatory M1 macrophage population induced by iron impairs wound healing in humans and mice. J. Clin. Invest. *121*, 985–997. https://doi.org/10.1172/JCI44490.
83. Ishida, Y., Kondo, T., Takayasu, T., Iwakura, Y., and Mukaida, N. (2004). The essential involvement of cross-talk between IFN-gamma and TGF-beta in the skin wound-healing process. J. Immunol. *172*, 1848–1855. https://doi.org/10.4049/jimmunol.172.3.1848.
84. Laato, M., Heino, J., Gerdin, B., Kähäri, V.M., and Niinikoski, J. (2001). Interferon-gamma-induced inhibition of wound healing *in vivo* and *in vitro*. Ann. Chir. Gynaecol. *90*, 19–23.
85. Shen, H., Yao, P., Lee, E., Greenhalgh, D., and Soulika, A.M. (2012). Interferon-gamma inhibits healing post scald burn injury. Wound Repair Regen. *20*, 580–591. https://doi.org/10.1111/j.1524-475X.2012.00812.x.
86. García, J.R., Quirós, M., Han, W.M., O'Leary, M.N., Cox, G.N., Nusrat, A., and García, A.J. (2019). IFN-gamma-tethered hydrogels enhance mesenchymal stem cell-based immunomodulation and promote tissue repair. Biomaterials *220*, 119403. https://doi.org/10.1016/j.biomaterials.2019.119403.
87. Kanno, E., Tanno, H., Masaki, A., Sasaki, A., Sato, N., Goto, M., Shisai, M., Yamaguchi, K., Takagi, N., Shoji, M., et al. (2019). Defect of Interferon gamma Leads to Impaired Wound Healing through Prolonged Neutrophilic Inflammatory Response and Enhanced MMP-2 Activation. Int. J. Mol. Sci. *20*, 5657. https://doi.org/10.3390/ijms20225657.
88. Cheng, M., and Hu, S. (2017). Lung-resident gammadelta T cells and their roles in lung diseases. Immunology *151*, 375–384. https://doi.org/10.1111/imm.12764.
89. Raulf, M., Liebers, V., Steppert, C., and Baur, X. (1994). Increased gamma/delta-positive T-cells in blood and bronchoalveolar lavage of patients with sarcoidosis and hypersensitivity pneumonitis. Eur. Respir. J. *7*, 140–147. https://doi.org/10.1183/09031936.94.07010140.
90. Lo Presti, E., Mocciaro, F., Mitri, R.D., Corsale, A.M., Di Simone, M., Vieni, S., Scibetta, N., Unti, E., Dieli, F., and Meraviglia, S. (2020). Analysis of colon-infiltrating gammadelta T cells in chronic inflammatory bowel disease and in colitis-associated cancer. J. Leukoc. Biol. *108*, 749–760. https://doi.org/10.1002/JLB.5MA0320-201RR.
91. Lo Presti, E., Di Mitri, R., Mocciaro, F., Di Stefano, A.B., Scibetta, N., Unti, E., Cicero, G., Pecoraro, G., Conte, E., Dieli, F., and Meraviglia, S. (2019). Characterization of gammadelta T Cells in Intestinal Mucosa From Patients With Early-Onset or Long-Standing Inflammatory Bowel Disease and Their Correlation With Clinical Status. J. Crohns Colitis *13*, 873–883. https://doi.org/10.1093/ecco-jcc/jjz015.
92. Xi, C., Jia, Z., Xiaoli, W., Na, Z., He, W., and Hao, J. (2019). New Aspect of Liver IL-17(+) gammadelta T Cells. Mol. Immunol. *107*, 41–43. https://doi.org/10.1016/j.molimm.2018.12.030.
93. Conroy, M.J., Mac Nicholas, R., Taylor, M., O'Dea, S., Mulcahy, F., Norris, S., and Doherty, D.G. (2015). Increased Frequencies of Circulating IFN-gamma-Producing Vdelta1(+) and Vdelta2(+) gammadelta T Cells in Patients with Asymptomatic Persistent Hepatitis B Virus Infection. Viral Immunol. *28*, 201–208. https://doi.org/10.1089/vim.2014.0133.
94. Beucke, N., Wesch, D., Oberg, H.H., Peters, C., Bochem, J., Weide, B., Garbe, C., Pawelec, G., Sebens, S., Röcken, C., et al. (2020). Pitfalls in the characterization of circulating and tissue-resident human gammadelta T cells. J. Leukoc. Biol. *107*, 1097–1105. https://doi.org/10.1002/JLB.5MA1219-296R.
95. Papalexi, E., and Satija, R. (2018). Single-cell RNA sequencing to explore immune cell heterogeneity. Nat. Rev. Immunol. *18*, 35–45. https://doi.org/10.1038/nri.2017.76.
96. Jaitin, D.A., Kenigsberg, E., Keren-Shaul, H., Elefant, N., Paul, F., Zaretsky, I., Mildner, A., Cohen, N., Jung, S., Tanay, A., and Amit, I. (2014). Massively parallel single-cell RNA-seq for marker-free decomposition of tissues into cell types. Science *343*, 776–779. https://doi.org/10.1126/science.1247651.
97. Shalek, A.K., Satija, R., Adiconis, X., Gertner, R.S., Gaublomme, J.T., Raychowdhury, R., Schwartz, S., Yosef, N., Malboeuf, C., Lu, D., et al. (2013). Single-cell transcriptomics reveals bimodality in expression and splicing in immune cells. Nature *498*, 236–240. https://doi.org/10.1038/nature12172.
98. Grover, A., Sanjuan-Pla, A., Thongjuea, S., Carrelha, J., Giustacchini, A., Gambardella, A., Macaulay, I., Mancini, E., Luis, T.C., Mead, A., et al. (2016). Single-cell RNA sequencing reveals molecular and functional platelet bias of aged haematopoietic stem cells. Nat. Commun. *7*, 11075. https://doi.org/10.1038/ncomms11075.
99. Kaluve, A.M., Le, J.T., and Graham, B.M. (2022). Female rodents are not more variable than male rodents: A meta-analysis of preclinical studies of fear and anxiety. Neurosci. Biobehav. Rev. *143*, 104962. https://doi.org/10.1016/j.neubiorev.2022.104962.
100. Zucker, I., Prendergast, B.J., and Beery, A.K. (2022). Pervasive Neglect of Sex Differences in Biomedical Research. Cold Spring Harbor Perspect. Biol. *14*, a039156. https://doi.org/10.1101/cshperspect.a039156.
101. Dalton, D.K., Pitts-Meek, S., Keshav, S., Figari, I.S., Bradley, A., and Stewart, T.A. (1993). Multiple defects of immune cell function in mice with disrupted interferon-gamma genes. Science *259*, 1739–1742. https://doi.org/10.1126/science.8456300.
102. Deskins, D.L., Ardestani, S., and Young, P.P. (2012). The polyvinyl alcohol sponge model implantation. J. Vis. Exp. *18*, 3885. https://doi.org/10.3791/3885.
103. Crane, M.J., Xu, Y., Henry, W.L., Jr., Gillis, S.P., Albina, J.E., and Jamieson, A.M. (2018). Pulmonary influenza A virus infection leads to suppression of the innate immune response to dermal injury. PLoS Pathog. *14*, e1007212. https://doi.org/10.1371/journal.ppat.1007212.
104. He, W., Hao, J., Dong, S., Gao, Y., Tao, J., Chi, H., Flavell, R., O'Brien, R.L., Born, W.K., Craft, J., et al. (2010). Naturally activated V gamma 4 gamma delta T cells play a protective role in tumor immunity through expression of eomesodermin. J. Immunol. *185*, 126–133. https://doi.org/10.4049/jimmunol.0903767.
105. Kadomoto, S., Izumi, K., and Mizokami, A. (2021). Macrophage Polarity and Disease Control. Int. J. Mol. Sci. *23*, 144. https://doi.org/10.3390/ijms23010144.
106. Kloc, M., Ghobrial, R.M., Wosik, J., Lewicka, A., Lewicki, S., and Kubiak, J.Z. (2019). Macrophage functions in wound healing. J. Tissue Eng. Regen. Med. *13*, 99–109. https://doi.org/10.1002/term.2772.
107. Ray, A., and Dittel, B.N. (2010). Isolation of mouse peritoneal cavity cells. J. Vis. Exp. *35*, 1488. https://doi.org/10.3791/1488.
108. Zhao, Y.L., Tian, P.X., Han, F., Zheng, J., Xia, X.X., Xue, W.J., Ding, X.M., and Ding, C.G.

(2017). Comparison of the characteristics of macrophages derived from murine spleen, peritoneal cavity, and bone marrow. J. Zhejiang Univ. - Sci. B *18*, 1055–1063. https://doi.org/10.1631/jzus.B1700003.

109. Starkey Lewis, P., Campana, L., Aleksieva, N., Cartwright, J.A., Mackinnon, A., O'Duibhir, E., Kendall, T., Vermeren, M., Thomson, A., Gadd, V., et al. (2020). Alternatively activated macrophages promote resolution of necrosis following acute liver injury. J. Hepatol. *73*, 349–360. https://doi.org/10.1016/j.jhep.2020.02.031.
110. Chen, W., Sandoval, H., Kubiak, J.Z., Li, X.C., Ghobrial, R.M., and Kloc, M. (2018). The phenotype of peritoneal mouse macrophages depends on the mitochondria and ATP/ADP homeostasis. Cell. Immunol. *324*, 1–7. https://doi.org/10.1016/j.cellimm.2017.11.003.
111. Ma, P.F., Gao, C.C., Yi, J., Zhao, J.L., Liang, S.Q., Zhao, Y., Ye, Y.C., Bai, J., Zheng, Q.J., Dou, K.F., et al. (2017). Cytotherapy with M1-polarized macrophages ameliorates liver fibrosis by modulating immune microenvironment in mice. J. Hepatol. *67*, 770–779. https://doi.org/10.1016/j.jhep.2017.05.022.
112. Enderlin Vaz da Silva, Z., Lehr, H.A., and Velin, D. (2014). *In vitro* and *in vivo* repair activities of undifferentiated and classically and alternatively activated macrophages. Pathobiology *81*, 86–93. https://doi.org/10.1159/000357306.
113. Martinez, F.O., Helming, L., Milde, R., Varin, A., Melgert, B.N., Draijer, C., Thomas, B., Fabbri, M., Crawshaw, A., Ho, L.P., et al. (2013). Genetic programs expressed in resting and IL-4 alternatively activated mouse and human macrophages: similarities and differences. Blood *121*, e57–e69. https://doi.org/10.1182/blood-2012-06-436212.
114. Rahal, O.M., Wolfe, A.R., Mandal, P.K., Larson, R., Tin, S., Jimenez, C., Zhang, D., Horton, J., Reuben, J.M., McMurray, J.S., and Woodward, W.A. (2018). Blocking Interleukin (IL)4- and IL13-Mediated Phosphorylation of STAT6 (Tyr641) Decreases M2 Polarization of Macrophages and Protects Against Macrophage-Mediated Radioresistance of Inflammatory Breast Cancer. Int. J. Radiat. Oncol. Biol. Phys. *100*, 1034–1043. https://doi.org/10.1016/j.ijrobp.2017.11.043.
115. Zhou, D., Ji, L., and Chen, Y. (2020). TSPO Modulates IL-4-Induced Microglia/Macrophage M2 Polarization via PPAR-gamma Pathway. J. Mol. Neurosci. *70*, 542–549. https://doi.org/10.1007/s12031-019-01454-1.
116. McWhorter, F.Y., Wang, T., Nguyen, P., Chung, T., and Liu, W.F. (2013). Modulation of macrophage phenotype by cell shape. Proc. Natl. Acad. Sci. USA *110*, 17253–17258. https://doi.org/10.1073/pnas.1308887110.

STAR★METHODS

KEY RESOURCES TABLE

REAGENT or RESOURCE	SOURCE	IDENTIFIER
Antibodies		
CD86 Polyclonal Antibody	Invitrogen	Catalog: PA5-88284
Anti-Mannose Receptor (206) antibody	Abcam	Catalog: ab64693
iNOS Polyclonal Antibody	Invitrogen	Catalog: PA1-036
Arginase 1 Polyclonal Antibody	Invitrogen	Catalog: PA5-29645
Lipopolysaccharides(LPS)	Solarbio	Catalog: L8880
Anti-mouse IFN-γ antibody	Selleck	Catalog: A2105
Brilliant Violet 605™ anti-mouse/human CD11b Antibody	Biolegend	Catalog: 101237
Anti-Vγ2 TCR antibody (equal to Vγ4 according to Tonegawa's nomenclature)	Bio X Cell	Catalog: BE0168 Clone: UC3-10A6
FITC anti-mouse Ly-6G Antibody	Biolegend	Catalog: 127605
Brilliant Violet 421™ anti-mouse Ly-6C Antibody	Biolegend	Catalog: 128031
Brilliant Violet 421 anti-mouse F4/80	Biolegend	Catalog: 123131
APC anti-mouse CD86 Antibody	Biolegend	Catalog: 105011
PE anti-mouse CD206 (MMR) Antibody	Biolegend	Catalog: 141706
PE anti-mouse TCR γ/δ Antibody	Biolegend	Catalog: 107507
APC anti-mouse TCR γ/δ Recombinant Antibody	Biolegend	Catalog: 111205
TCR V gamma 2 Monoclonal Antibody	Invitrogen	Catalog: 46-5828-82
FITC anti-mouse TCR Vγ2 Antibody	Biolegend	Catalog: 137703
PE anti-mouse IFN-γ Antibody	Biolegend	Catalog: 505807
Chemicals, peptides, and recombinant proteins		
Recombinant Mouse IL-4 Protein	Abclonal	Catalog: RP01161
Recombinant Mouse Interferon γ/IFN-γ/IFN-gamma	Solarbio	Catalog: P00564
Active Recombinant Mouse CSF-1/M-CSF Protein	Abclonal	Catalog: RP01216

RESOURCE AVAILABILITY

Lead contact

Further information and requests for resources and reagents should be directed to and will be fulfilled by the lead contact, Dr Weifeng He (heweifeng@tmmu.edu.cn).

Materials availability

This study did not generate new unique reagents.

Data and code availability

- All data reported in this paper will be shared by the lead contact upon request. This paper does not report original code. Any additional information required to reanalyze the data reported in this paper is available from the lead contact upon request.

EXPERIMENTAL MODEL AND STUDY PARTICIPANT DETAILS

Mouse lines

C57BL/6J wildtype (WT) mice were purchased from Beijing Vital River Laboratory Animal Technology Co., Ltd. C57 B6.129S7-Ifngtm1Ts/J (IFN-$\gamma^{-/-}$) mice were obtained from Ji'nan University, which were purchased from The Jackson Laboratory (Bar Harbor, ME). These mice were generated by the insertion of a neomycin gene into exon 2, which introduced a termination codon after the first 30 amino acids of the mature protein.[101] Heterozygous offspring were intercrossed to generate homozygous mice. All mice were housed in specific pathogen-free facilities. Male mice aged 6-8 weeks were used for all experiments. The experimental procedures were approved by the Institutional Animal Care and Use Committee and met the requirements of the Ethics Committee of Army Military Medical University.

METHOD DETAILS

Antibody-mediated Vγ4 T cells depletion

Mice received intraperitoneal injection of anti-Vγ4 TCR antibody (UC3-10A6, Bio X Cell, USA) or IgG isotype control antibody (BE0260; Bio X Cell) at a dose of 450 μg 7 days before wounding. The efficiency of Vγ4 T cells depletion in different tissues was verified by flow cytometry.

Full-thickness excision wound model

Dorsal fur was removed 1 day before wounding. The next day mice (18-20g) were anaesthetized by isoflurane inhalation and the exposed skin was sterilized with 75% alcohol. With a 6 mm diameter biopsy punch, one full-thickness excisional wound extending through the panniculus carnosus was generated on each side of the dorsal midline per mouse by a hole puncher. Wounds were left uncovered without a dressing. Their area was recorded macroscopically contrasting to a standard silicon ring on the 2^{nd}, 4^{th}, 6^{th} and 8^{th} days post injury, the residual percentage was measured and calculated using Image-Pro Plus 6.0 software, USA) based on the photographs recorded. The formula to compute percentage is: residual area (%) = WAr/WAi × 100%, where WAr represents the residual wound area on the indicated timepoints, and WAi represents the initial wound area.

Sponge implantation model

After removing dorsal fur 1 day before, two transverse full-thickness incisions (1 cm) were made on each side of the dorsal midline, and a bloodless subcutaneous pocket underneath each wound was established, into which a Polyvinyl Alcohol (PVA) sponge (6-mm diameter, 2-mm thick; Jian De Kang Hua Medical Devices Co., LTD, Medical PVA, China) was implanted through the skin incision,[42,102,103] which was subsequently closed by a 5-0 surgical suture needle with thread (NingBo Medical Needle Co., LTD, China). To observe the interaction between Vγ4 T cells and macrophages in sponges *in situ*, wound tissues with the sponge were harvested on the 2^{nd} and 4^{th} days post sponge implantation, which were immediately fixed, paraffin-embedded, and sectioned.

Isolation and culture of Vγ4 T cells

The PVA sponges were taken aspetically from the mice aseptically on the 2^{nd} day post implantation and placed into Phosphate-buffered saline (PBS), they were then minced into tiny pieces and passed through a 70-μm cell strainer to get single-cell suspensions. Subsequently, these cells were washed in PBS and separated by a lymphocyte separation medium (Cedarlane, CL5031, Canada) according to the manufacture's instruction. Later, the collected cells were re-suspended with RPMI1640 media containing fetal bovine serum (FBS) (Gibco, 10099141C, Australia) and interleukin-2 (IL-2) (R&D, BT-015, USA) and cultured for 7 days,[104] cells were cultured with plate-coated anti-Vγ4 antibody, in the first 3 days, the suspended cells were collected and transferred into another plate (coated anti-Vγ4 antibody) every day, and identification of the Vγ4 T cells was conducted by flow cytometry using the APC-anti-Vγ4 (Biolegend, 118115, USA) antibody, and immunofluorescence using PE-anti-γδ (Biolegend, 118108, USA), FITC-anti-Vγ4 (Biolegend, 137703, USA) and Hochest (Beyotime, 33258, China). The purity of the Vγ4 population was >90%.

Isolation and culture of Bone Marrow Derived Macrophages (BMDMs)

Bone marrow cells were isolated from the long bones of mice (femurs and tibias), and the bone marrow was flushed out with PBS and filtered through a 70 μm cell strainer, the obtained cells were cultured in RPMI1640 media with 10% FBS for 6 days, macrophage colony-stimulating factor (M-CSF) (20 ng/ml, Abclonal, RP01216, China) was added into the media to stimulate the differentiation of the cells into BMDMs for 6 days, the matured BMDMs were recognized to be the M0 unstimulated naïve macrophages.[105,106] M0 macrophages were always derived from bone marrow or peritoneal lavage,[107–110] though they are inadequate to reflect macrophage heterogeneity, their representation of the unchallenged state of macrophages makes them the ideal subject for *in vitro* study, and thus they have been applied in various studies.[111–113] Identification of the macrophages was conducted by flow cytometry using the FITC-anti-F4/80 antibody (Biolegend, 123108, USA) and immunofluorescence using FITC-anti- F4/80 and Hoechst. The purity of BMDMs was >95%.

Co-culture of the cells

Matured BMDMs (MΦ) were enzymatically digested with trypsin for 5 mins, RPMI1640 media with 10% FBS was added to stop digestion, and cell pellets were re-suspended with a pipette. After centrifugation, the macrophages were re-suspended with RPMI1640 (containing M-CSF and 5% FBS), which were then transferred into a sterile 24-well plate, approximately 5×10^5 cells per well. One hour later, cultured Vγ4 T cells were also seeded into the plate and co-cultured with MΦ at a 1:1 ratio, the temperature of the incubator was set to be 37°C. To observe the function of Vγ4 T cells in modulating M1 polarization, lipopolysaccharide (LPS) (Solarbio, L8880, China) was added into the media at a concentration of 100 ng/mL.[114] To observe their function in modulating M2 polarization, interleukin-4 (IL-4) (Abclonal, RP01161, China) was added into the media at a concentration of 40 ng/mL.[115] To evaluate the effect of Vγ4 T cells on regulating the transformation of M1 to M2, the MΦ were firstly induced to M1 with LPS (100 ng/mL) and IFN-γ (40 ng/mL, Solarbio, P00564, China) for 24 hours, later, the M1 macrophages were co-cultured with Vγ4 T cells at the indicated ratio.[114,116] To verify the influence of IFN-γ secreted by Vγ4 T cells on macrophages polarization, an IFN-γ neutrolizer (Selleck, A2105, USA) was added into the co-culture media at a concentration of 10μg/ml. All co-cultures were conducted in anoxic incubator (1% oxygen) to simulate the ischemic and hypoxic environment during wound repair. Twenty-four hours later, macrophages or Vγ4 T cells were harvested and analyzed by flow cytometry and immunofluorescence for markers and cytokines. For analyzing

intracellular staining, Cyto-FastTM Fix/Perm Buffer Set (Biolegend, 426803, USA) was used for cell fixation and perforation. For cytokine analysis of macrophages, a Brefeldin A Solution (Biolegend, 420601, USA) was added into media 4 hours before terminating the co-culture (1:1000). For cytokines of Vγ4 T cells, a Cell Activation Cocktail (with Brefeldin A) (Biolegend, 423303, USA) was added (1:500).

Transfer of Vγ4 T cells

To explore the effect of Vγ4 T cells, *Vγ4 T cells* from wildtype (WT) or IFNγ$^{-/-}$ mice were transferred by intradermal injection around wounds from day 1 to day 3 post wounding, 5×10^5 Vγ4 T cells (>90% purity upon re-analysis) were transferred at each time point. For tracing Vγ4 T cells *in vivo*, cells were labeled in advance with DiI-Red (Beyotime, C1036, China) or DiO-Green (Beyotime, C1038, China) *in vitro* and were transferred into mice body by intradermal injection or intravenous injection on the 2nd day post injury (1×10^6 Vγ4 T cells), 24 hours later, these cells were detected by flow cytometry and immunofluorescence among different tissues. For wound tissues and lymph nodes, immunofluorescence identification was conducted on frozen section, while for blood and bone marrow, collected cells were analyzed.

Hematoxylin and eosin (H&E) staining

Wounded mice were euthanized with an intraperitoneal injection of 1% pentobarbital (1 mL/mice). The wound tissues were then harvested on the 2nd, 4th, 6th and 8th days post skin excision, which were immediately fixed, paraffin-embedded, and sectioned. Subsequently, the sections were deparaffinized, hydrated and stained with hematoxylin and eosin (H&E), the whole dyeing process includes five steps: dewaxing, dyeing, dehydration, transparency and sealing. The length of the neo-epidermis, the thickness and area of the granulation tissue were recorded under a full slide scanning microscope (VS200, Olympus, Japan), and then were analyzed using IPP 6.0 software.

Immunohistochemical staining

The paraffin sections of the wound were deparaffinized, hydrated and blocked in turn, and then incubated with the primary antibody at 37°C for two hours. Later, they were incubated with reaction enhencer (ZSGB-BIO, PV900, China) for 20 minutes and followed by an incubation of an enhenced enzyme-labeled goat anti-mouse/rabbit IgG antibody (ZSGB-BIO, PV900, China) for 30minutes at room temperature. Subsequently, the counterstaining was carried out with hematoxylin (Beyotime, China) and the slices were photographed under a full slide scanning microscope (Olympus, Japan). The primary antibodies were as the follows: anti-IFN-γ (1:200) (NOVUS, NBP2-66900, USA), anti-TNF-α (1:200) (Abcam, ab1793, UK), anti-IL-6 (1:200) (Abclonal, A0286, China), anti-IL-10 (1:200) (Invitrogen, ARC9102, USA) and anti-TGF-β (1:200) (Proteintech, 21898-1-AP, USA).

Immunofluorescence microscopy

The wound paraffin slides mentioned above were deparaffinized according to the standard procedure, they were firstly put into dimethylbenzene for 10 mins and then transferred into alcohol with reduced gradient concentration (100% for 10 mins, 95% for 3 mins, 85% for 3mins and 75% for 2 mins), later they were moved into distilled water for 5 mins, antigens were retrieved by boiling in sodium citrate buffer (10 mM, pH 6.0). Samples were blocked with goat serum and permeabilized with Triton (Beyotime, P0096, China), then incubated with primary antibodies overnight at 4°C, followed by secondary antibody incubation. Slides were counterstained with DAPI (Beyotime, P0131, China) and covered with coverslips. Frozen section samples didn't need deparaffinization, and the staining procedure was identical to that of of paraffin slide.

For cell culture samples, a cover glass was placed into each well of the plate in advance, after the corresponding treatment, supernatants were discarded, and the cover glasses were washed with PBS, fixed with 4% paraformaldehyde (Beyotime, P0099, China). Later, they were stained according to the standard procedure identical to the tissue slides. In identifying the DiI-labelled Vγ4 T cells of bone marrow and blood by immunofluorescence, collected cells were stained with Hoechst before photographing.

All slides were photographed on a Zeiss LSM 880 confocal microscope and analyzed using ImageJ software. The main antibodies were listed below: anti-F4/80 (1:500) (Invitrogen, MA1-91124, USA), anti-CD86 (1:500) (Invitrogen, PA5-88284, USA), anti-CD206 (1:500) (Abcam, ab64693, UK), anti-iNOS (1:500) (Invitrogen, PA1-036, USA), anti-Arg-1 (1:500) (Invitrogen, PA5-29645, USA), anti-Vγ4 (1:500), the anti-TNF-α, anti-IL-6, anti-IL-10 and anti-TGF-β were the same as the antibodies mentioned above. Goat anti-Rabbit IgG (Invitrogen, A-11034, USA), Donkey anti-Rabbit IgG (Invitrogen, A-31572, USA), Goat anti-rat IgG (Biolegend, 405420, USA), Goat anti-rat IgG (Invitrogen, A-11006, USA), Goat anti-Mouse IgG (Invitrogen, A-21236, USA), Goat anti-Armenian hamster IgG (Abcam, ab173004, UK).

Flow cytometry analysis of cells and intracellular cytokine staining

Skin tissues which are less than 2 mm away from wound edge were harvested on indicated days. After weighing, they were cut into tiny pieces and digested with RPMI1640 media containing 5 mg/ml collagenase IV (Worthington Biochem), 10 U/ml DNase I (Stemcell Technologies) and 5% FBS at room temperature. After two hours of shaking, the cell suspensions were passed through 70 μm strainers to remove impurities. Later, cells were counted with a hemocytometer, incubated with CD16/CD32 Fc block (Biolegend, 101319, USA) and then stained with the related anti-mouse antibodies. For analyzing cytokines, obtained cells were re-suspended with RPMI1640 containing 10% FBS and a Cell Activation Cocktail (with Brefeldin A), and then cultured in an incubator for 5 hours. Data were acquired on a CytoFlex (Beckman) or Fortessa X-20 (BD Biosciences) and analyzed using FlowJo software. The main antibodies were listed below: anti-CD11b (Biolegend, 101237, USA), anti-Ly6G (Biolegend, 127605, USA), BV421 anti-Ly6C (Biolegend, 128031, USA), BV421 anti-F4/80 (Biolegend, 123131, USA), APC anti-CD86 (Biolegend, 105011, USA), PE anti-CD206 (Biolegend, 141706, USA), BV510 Anti-CD3 (Biolegend, 100233, USA), BV605 Anti-CD3 (Biolegend,

100237, USA), PE anti-γ/δ TCR (Biolegend, 107507, USA), APC anti-γ/δ TCR (Biolegend, 111205, USA), APC anti-Vγ1 TCR (Biolegend, 141107, USA), ef710 anti-Vγ4 TCR (Invitrogen, 46-5828-82, USA), FITC anti-Vγ4 TCR (Biolegend, 137703, USA), PE anti-IFN-γ (Biolegend, 505807, USA).

Blood samples were collected by cardiac puncture on indicated days, leukocytes were isolated from whole blood using a mouse peripheral blood mononuclear cell isolation fluid (Tianjin Haoyang Biological Manufacture Co., Ltd) according to the manufacturer's instruction, the staining items were similar to those used with the wound tissue cells except for staining with F4/80, CD86 and CD206.

Lymph nodes were also dissected, mechanically dissociated, and passed through 70 μm strainers to obtain single cell suspensions. Their staining scheme was the same as that of blood sample. Bone marrow cells were obtained according to the procedure mentioned above, cells were stained according to the same staining scheme and then were also analyzed by flow cytometry.

For cultured macrophages and Vγ4 T cells, they were collected as the procedure mentioned above after the corresponding treatment, and then stained as per the routine staining procedure.

Western blot

Briefly, cells or wound tissues were lysed with ice-cold 1×RIPA (Radio Immunoprecipitation Assay) lysis buffer containing protease/phosphatase inhibitors (Beyotime, P1005, China), a total of 20 μg protein for each specimen was resolved by standard SDS-PAGE electrophoresis and transferred electrophoretically to polyvinylidene difluoride membranes. After blocking, membranes were incubated with primary antibodies overnight at 4°C, followed by horseradish peroxidase (HRP)-conjugated secondary antibodies (Beyotime, China) and chemiluminescent substrate development. The main primary antibodies used include anti-CD86 (1:500), anti-CD206 (1:500), anti-iNOS (1:500), anti-Arg-1 (1:500), anti-TNF, anti-IL-6, anti-IL-10 and anti-TGF-β which were the same as the antibodies mentioned above. Band intensities were quantified using ImageJ.

Quantitative real-time PCR

RNA was extracted using TRIzol reagent (Thermo Fisher Scientific, A33254, USA) and reverse transcription was performed to obtain cDNA using reverse transcription kit (Bioground, BG0070, China). Real-time PCR was performed using PowerUp SYBR Green Master Mix (RR820A, Takara) to evaluate the gene expression of iNOS, TNF-α, Arg-1, Ym1/2 and Fizz1. Relative gene expression was calculated using the 2-ΔΔCT method.

ELISA assay

For cultured cells, the supernatants were collected, they were centrifuged at 8,000g for 10 minutes. ELISA was performed for IFN-γ (AiFang biological, AF2182-A, China) according to the manufacturer's protocol. Absorbance was measured using a microplate reader.

QUANTIFICATION AND STATISTICAL ANALYSIS

Data are presented as the Mean ± SD. Statistical tests were performed using GraphPad Prism (GraphPad Software, San Diego, CA, USA). Differences between two groups were assessed by an unpaired Student's t-test. One-way ANOVA with Tukey's test was used for comparisons of three or more groups. Levene's Test was used to compare equality of variances. P values <0.05 were considered statistically significant.